Contrib Mineral Petrol (1997) 128: 176–196

Jean-Marc Montel · Daniel Vielzeuf

Partial melting of metagreywackes, Part II. Compositions of minerals and melts

Received: 11 July 1995 / Accepted: 27 February 1997

Abstract A series of experiments on the fluid-absent melting of a quartz-rich aluminous metagreywacke has been carried out. In this paper, we report the chemical composition of the phases present in the experimental charges as determined by electron microprobe. This analytical work includes biotite, plagioclase, orthopyroxene, garnet, cordierite, hercynite, staurolite, gedrite, oxide, and glass, over the range 100–1000 MPa, 780–1025 °C. Biotites are Na- and Mg-rich, with Ti contents increasing with temperature. The compositions of plagioclase range from An_{17} to An_{35}, with a significant orthoclase component, and are always different from the starting minerals. At high temperature, plagioclase crystals correspond to ternary feldspars with Or contents in the range 11–20 mol%. Garnets are almandine pyrope grossular spessartine solid solutions, with a regular and significant increase of the grossular content with pressure. All glasses are silicic (SiO_2 = 67.6–74.4 wt%), peraluminous, and leucocratic (FeO + MgO = 0.9–2.9 wt%), with a bulk composition close to that of peraluminous leucogranites, even for degrees of melting as high as 60 vol.%. With increasing pressure, SiO_2 contents decrease while K_2O increases. At any pressure, the melt compositions are more potassic than the water-saturated granitic minima. The H_2O contents estimated by mass balance are in the range 2.5–5.6 wt%. These values are higher than those predicted by thermodynamic models. Modal compositions were estimated by mass balance calculations and by image processing of the SEM photographs. The positions of the 20 to 70% isotects (curves of equal proportion of melt) have been located in the pressure-temperature space between 100 MPa and 1000 MPa. With increasing pressure, the isotects shift toward lower temperature between 100 and 200 MPa, then bend back toward higher temperature. The melting interval increases with pressure; the difference in temperature between the 20% and the 70% isotects is 40 °C at 100 MPa, and 150 °C at 800 MPa. The position of the isotects is interpreted in terms of both the solubility of water in the melt and the nature of the reactions involved in the melting process. A comparison with other partial melting experiments suggests that pelites are the most fertile source rocks above 800 MPa. The difference in fertility between pelites and greywackes decreases with decreasing pressure. A review of the glass compositions obtained in experimental studies demonstrates that partial melting of fertile rock types in the crust (greywackes, pelites, or orthogneisses) produces only peraluminous leucogranites. More mafic granitic compositions such as the various types of calk-alkaline rocks, or mafic S-type rocks, have never been obtained during partial melting experiments. Thus, only peraluminous leucogranites may correspond to liquids directly formed by partial melting of metasediments. Other types of granites involve other components or processes, such as restite unmixing from the source region, and/or interaction with mafic mantle-derived materials.

J.-M. Montel (✉) · D. Vielzeuf
CNRS, UMR 6524 "Magmas et Volcans",
Université Blaise Pascal,
5 rue Kessler, F-63000 Clermont-Ferrand, France

Editorial responsibility: W. Schreyer

Introduction

The generation and ascent of granitic magmas are among the most important geodynamic processes as they represent efficient mechanisms for transporting heat and low-density materials (granitic melt) toward the surface of the Earth. They provide means to restore thermal and mechanical equilibria in the lithosphere, after disturbances created by processes such as subduction or continental collision (Vielzeuf et al. 1990). Intra-crustal granitic magmatism is possible only if appropriate source rocks are present. Among a variety of different protoliths, metapelites and metagreywackes can be considered as potential sources for granitic magmas as they contain water and quartzo-feldspathic components necessary to produce liquids of granitic composition.

Clemens and Vielzeuf (1987) presented a method for estimating the volume of melt for fluid-absent melting using a mass balance approach and models of water solubility in alumino-silicate melts (Burnham 1979; Burnham and Nekvasil 1986). This method is applicable only when the amount of water in the hydrate is the limiting factor for melting, and after total breakdown of biotite or amphiboles. Since the pioneering experimental work of Winkler (1957) and Wyart and Sabatier (1959), it is accepted that partial melting of felsic metamorphic rocks produces liquids with granitic compositions. In the absence of satisfactory thermodynamic models, experimental determination of the proportion and composition of melts formed through the anatexis of crustal rocks still provides a fundamental contribution to understanding the granite genesis. As emphasized by Johannes and Holtz (1990) and Joyce and Voigt (1994), the question of the quantities of FeO, MgO and excess alumina (normative corundum) that can be incorporated in an anatectic melt is still matter of discussion.

This paper presents and discusses analyses of the products of partial melting experiments from a quartz-rich metagreywacke. It complements previously published phase equilibrium data (Vielzeuf and Montel 1994a). The starting rock contains 41 wt% quartz, 32 wt% plagioclase (An_{22}-Or_{02}-Ab_{76}), and 25 wt% biotite (X_{Fe} = 0.56, Al_2O_3 = 19.51 wt%, TiO_2 = 2.80 wt%), with accessory apatite, zircon, monazite, tourmaline, and pyrite. Pressure and temperature conditions of crystallisation of this rock have been estimated as 200–300 MPa, 670–720 °C (Montel et al. 1992). To check for thermodynamic equilibrium during the experiments, two types of starting materials were used: a very fine rock powder (grain size < 5 μm) and a glass of the same bulk composition (including water and FeO) obtained by melting the powder at 300 MPa, 1300 °C for 30 minutes in a sealed platinum capsule. Experiments carried out with the rock powder will be referred to as "melting experiments", and those carried out with the glass "crystallisation experiments". Experimental techniques and capsule configurations are outlined in detail in Vielzeuf and Montel (1994a). In this study, pressure ranges from 100 MPa to 2 GPa (1–20 kbar), while temperature encompasses the entire range from the appearance of orthopyroxene to the disappearance of biotite as determined by Vielzeuf and Montel (1994a). No precise estimate of the oxygen fugacity (FO_2) was possible as runs were carried out under fluid-absent conditions. However, the intrinsic oxygen fugacities, determined experimentally by solid buffers, are close to Ni-NiO buffer (NNO) for the externally heated pressure vessels, and close to MnO-Mn_3O_4 for the internally heated pressure vessel. The intrinsic oxygen fugacity of the piston cylinder is probably more reducing, but no direct measurement was made.

All run products contained quartz and plagioclase. The following phases were present in most experiments: glass, biotite (Bt), orthopyroxene (Opx), and Fe-Ti oxides, plus cordierite (Crd) at 100–300 MPa and garnet (Grt) at higher pressure. Gedrite, staurolite, and Al-spinel (Spl) were also found in some runs. K-feldspar (Kfs) is not present as a discrete phase, but orthoclase (Or) solid solution with plagioclase is observed. The compositions of each phase from each charge were determined over the range 100–1000 MPa.

In part I of the study (Vielzeuf and Montel 1994a), the phase assemblages were interpreted to result from different model reactions. One of the most important is

$$(\mathrm{I})\ \mathrm{Bt} + \mathrm{Pl} + \mathrm{Qtz} \Longleftrightarrow \mathrm{Opx} + \mathrm{Grt/Crd/Spl} + \mathrm{Kfs} + \mathrm{melt}$$

(*Bt* biotite, *Pl* plagioclase, *Qtz* quartz, *Opx* orthopyroxene, *Grt* garnet, *Crd* cordierite, *Spl* Spinel, *Kfs* K-feldspar) as predicted from different petrogenetic models (Thompson 1982; Clemens 1984; Grant 1985; Vielzeuf and Holloway 1988). Our experimental results clearly indicate that this reaction, limited in the pressure-temperature plane by the Opx-in and Bt-out curves, occurs at a higher temperature than commonly considered (Clemens 1984). In addition, the experiments indicated the importance of another model reaction:

$$(\mathrm{II})\ \mathrm{Bt} + \mathrm{Pl} + \mathrm{Qtz} \Longleftrightarrow \mathrm{Grt} + \mathrm{Kfs} + \mathrm{melt}$$

This reaction corresponds to a huge multivariant field with a low $\mathrm{d}P/\mathrm{d}T$ slope which explains the progressive replacement of biotite by garnet with increasing pressure at a given temperature.

Analytical and mass balance calculation procedures

Electron microprobe analysis

Analyses were carried out using a Cameca Camebax electron microprobe at Université Blaise Pascal, Clermont-Ferrand. Operating conditions were 15 kV accelerating voltage, and a 10 nA sample current. The counting times were 10 seconds on peak and 5 seconds on the background. Three spectrometers were used simultaneously with Na and K analysed first to minimise losses. The following standards were used for calibration: natural albite (Na, Si), orthoclase (K), olivine (Mg), and wollastonite (Ca), synthetic Fe_2O_3 (Fe), Al_2O_3 (Al), and $MnTiO_3$ (Mn, Ti). The ZAF correction procedures were applied. The errors related to the counting statistics at the 95% confidence level (Ancey et al. 1978) have been determined for each element for some typical compositions and are reported in Table 1. An estimate of the excited volumes for Na (maximum size) and Fe (minimum size) calculated according to Castaing (1960) are given also. Because of the small size of the phases, considerable difficulties were encountered. As distinction of the phases by direct (optical) observation of the carbon-coated surface was not possible, backscattered electron imaging was used. Three main analytical difficulties were encountered:

1. *Size of the phases*: some of them are so small (typically less than 5 μm) that special care was required to avoid contamination by the surrounding phases. This is particularly problematic at low pressures because the phases are noticeably smaller (Vielzeuf and Montel 1994a). This is true for orthopyroxene because of its acicular shape, for biotite (too thin), and for oxide minerals (very small). The problem also exists for garnet, which is always riddled with quartz inclusions. The following criteria were used to select reliable analyses. For biotite: SiO_2 contents close to or lower than 40 wt%, no CaO, K_2O higher than 8 wt%, and oxide totals close to 96 wt%. For orthopyroxene: SiO_2 lower than 50 wt%, low K_2O and Na_2O contents, oxide total approaching 100%; oxygen close to or lower than 6 on a 4-cation basis in the structural formula and

Table 1 Typical analytical errors. Absolute errors for electron microprobe analyses, calculated from the statistical model of Ancey et al. (1978). *Vol. Na* and *Vol. Fe* are the diameter, in μm, of the excited volumes for sodium and iron respectively, calculated following Castaing (1960). (*Pl* plagioclase, *Opx* orthopyroxene, *Crd* cordierite, *Bt* biotite, *Grt* garnet, *Hc* hercynite)

	glass	Pl	Opx	Crd	Bt	Grt	Hc
SiO_2	0.73	0.67	0.58	0.65	0.56	0.54	0.22
Al_2O_3	0.23	0.33	0.24	0.38	0.32	0.34	0.55
FeO	0.15	0.12	0.66	0.33	0.44	0.68	0.85
MgO	0.05	0.04	0.35	0.24	0.28	0.23	0.25
MnO	0.09	0.16	0.14	0.11	0.10	0.22	0.13
CaO	0.08	0.21	0.06	0.07	0.15	0.13	0.06
Na_2O	0.13	0.28	0.08	0.07	0.18	0.05	0.17
K_2O	0.17	0.10	0.05	0.06	0.26	0.05	0.06
TiO_2	0.10	0.08	0.11	0.11	0.20	0.12	0.10
Vol. Na	2.9	2.5	1.8	2.5	2.3	1.7	1.5
Vol. Fe	2.2	1.9	1.4	2.0	1.8	1.3	1.2

charge balance close to 0. For garnet: SiO_2 close to 40 wt%, no K_2O or Na_2O, oxide total close to 100%. For plagioclase: low MgO or TiO_2, oxide total close to 100%. In the exceptional cases where only contaminated compositions were available, we applied a correction procedure. The amount of contamination was determined on the basis of the elements that should be absent in the contaminated phase and abundant in the contaminating phase (e.g. Ca in biotite, K in orthopyroxene). After correction, the new values were normalized to ideal totals, e.g. 100% for orthopyroxene or 96% for biotite. This procedure provided satisfactory results as long as the amount of contamination was lower than 10%. No objective criteria could be used for the glass compositions, but contamination by plagioclase was indicated by anomalously high Ca and Na contents. Glass contamination by quartz and cordierite was more difficult to detect, except in case of anomalously high SiO_2 values (quartz), or Al_2O_3 (cordierite). Such compositions were rejected.

2. *Phase identification*: some phases are difficult to distinguish from each other. This is mainly true for quartz, glass, plagioclase, and cordierite. Where necessary, identification was carried out by EDS (energy dispersive spectroscopy) analysis. However, this was not possible for glasses as even short EDS analysis could induce important alkali losses. Therefore, glass analyses were made directly, after careful examination of the backscattered electron image.

3. *Loss of alkalis*: A particular problem for glass analysis concerned Na and K migrations under the electron beam. Solutions commonly used to circumvent this problem, such as beam defocussing or displacement could rarely be used due to the small size of the glass pools. As far as possible, 1.5×1.5 μm or 4×4 μm electron beams, instead of a fully focussed beam, were used. However this was not sufficient to avoid alkali migration, and a correction procedure was employed. A series of measurements were performed on the starting glass *CEVG* (1.43 wt% H_2O) and on a water-saturated glass, free of crystals, made from *CEVP* at 270 MPa (7 wt% H_2O). These showed that, for a given intensity of beam current, only Na and K were affected by losses. The correction factor for Na and K depended on the water content of the glass, and on the size of the analysed area. A formulation for the correction factor was established with the additional assumption that no correction was necessary for water-free glasses. However, as the water contents in our experimental glasses are unknown, we used an iterative procedure. First, a mass balance calculation (determination of the modal proportions of the phases) was made using the uncorrected values for Na_2O and K_2O. It provided a first estimate of the water content of the glasses and of the correction factors for Na and K. Then a new mass balance calculation was performed, using the new values for Na_2O and K_2O. The procedure was repeated until the system of equations converged.

Mineral compositions are given in Tables 2–6, and some representative structural formulae are given in Table 7. The glass compositions are given in Table 8. These allow the modal proportions of the minerals and glass in each charge to be estimated by mass balance.

Mass balance procedure

Mass balance calculations were carried out during the correction procedures for Na and K in the glasses, using a global block-wise inversion (Albarède and Provost 1977; Provost 1989), with the analytical errors given in Table 1 as 2σ. Results are shown in Table 9. When a phase composition was unavailable, the composition of the same phase at the closest possible pressure-temperature conditions was used. This is justified by the fact that within a small *P-T* interval, most phases show progressive and limited compositional variations.

Mass balance calculations yield reliable results only if the system remains chemically closed during the experiment. With the experimental techniques used here, some iron from the sample can be lost to the Au container, and hydrogen can diffuse through the capsule walls. Iron losses in precious metal are well documented in platinum at high temperature, but are not important in gold, as shown by Puziewicz and Johannes (1990). The amount of hydrogen that diffused through the capsule walls can be estimated from the amount of iron that has been oxidised during the experiments. In the starting material, 90 mol% of iron is Fe^{2+} (Vielzeuf and Montel 1994a). The structural formulae of the minerals indicate that Fe^{3+} is a major component only in oxide minerals. Therefore, an estimate of the Fe^{3+} content in the charge, after the run, can be made from the oxide mineral content (2–3 wt%), assuming that it is all magnetite. The Fe^{3+} content of the melt is neglected because of the low Fe contents of the glasses. This calculation indicates that a maximum of 40 mol% of Fe is Fe^{3+}, which corresponds to a maximum relative loss of 12% water contained in the sealed capsule through hydrogen diffusion during the runs. Thus, water contents of the glasses, may be overestimated by the same proportion (12% relative). The effect of this uncertainty on the alkali-loss correction factors can be neglected, as well as the effect on the calculated proportions of glass and hydrous minerals, because water is not considered in the mass balance calculation. Also, the composition of the melt could be modified during the quench. Quenching times depend on the technique used. This varies from a few seconds in the piston cylinders, to 100 s in the externally heated pressure vessels and two minutes in the internally heated pressure vessels. However, textural and compositional evidence for quenching effects was not observed.

In order to test the validity of the mass balance procedure, we estimated the crystal/glass proportions directly from back scattered electron images. Because of the textural homogeneity of the charges, and the small size of the crystals, a single representative view at 2000 magnification (2200 μm^2) of most charges was used. Each image was redrawn by hand to enhance the contrast between glass and crystals. The final glass/crystals ratio was obtained by image processing using *Visilog* software. Because of the heterogeneous grain size in the crystallisation experiments (see Fig. 1D in Vielzeuf and Montel 1994a), this was carried out only on the charges from the melting experiments. The melt proportion obtained by image processing is usually slightly lower than the proportion calculated

by mass-balance (Table 9). This discrepancy can be explained partly by the presence of a thin layer of melt along grain boundaries (Laporte 1994, therein Figs. 8 and 9a, b). These thin films cannot be seen in backscattered electron SEM views.

Attainment of equilibrium

The euhedral shape and the homogeneous size of the crystals in the melting experiments, together with the regular distribution of melt, indicate that textural equilibrium was approached during the experiments. The fact that both biotite and plagioclase compositions are different from those of the starting material (see below), indicates that the material was reactive enough to reach new compositions within run durations of about 15 days. For biotite, garnet, cordierite and glass, compositions in melting and crystallisation experiments are very close, indicating that chemical equilibrium was approached. Plagioclase compositions are more scattered due to imperfect attainment of equilibrium, or analytical problems. We favour the second hypothesis because the composition of the plagioclase in the charges is always different from that of the starting plagioclase, plagioclase crystals do not appear zoned, and they display perfect euhedral equilibrium textures. In contrast, orthopyroxene displays some characteristic disequilibrium features such as grain to grain chemical variations and zoning in Al_2O_3. Natural orthopyroxenes in granites never have such high Al_2O_3 contents. We think that kinetics favour the formation of Al-rich metastable crystals in the early stages of the experiment and that the sluggish diffusion of Al prevents subsequent re-equilibration. Similar difficulties are documented for clinopyroxene in basaltic systems.

Analytical results

Mineral compositions

Biotite (Table 2) is one of the most common phases, present at all run pressures, and disappearing at high temperature. All are more magnesian and less aluminous than the starting biotite. The Na_2O contents are high (0.5–1.2 wt%), and TiO_2 is variable. Such compositions are similar to those obtained by Conrad et al. (1988), with a starting material comparable in terms of X_{Fe}. They are more magnesian than biotites analysed by Patiño-Douce et al. (1993), and Holtz and Johannes (1991) who used a starting material with higher $X_{Fe.}$ The biotite compositions reported by Patiño-Douce et al. (1993) are also significantly richer in Al_2O_3, probably because Al-silicate is present in their experiments. Biotite TiO_2 contents are positively correlated with temperature (Fig. 1), a common feature documented experimentally for phlogopite (Robert 1976). Two trends can be distinguished: a high-Ti trend for the experiments containing a Fe-Ti oxide, and a low-Ti trend for the other runs. The general features are compatible with data of Conrad et al. (1988) and Patiño-Douce et al. (1993).

Orthopyroxene (Table 3) is present in many experiments. Aluminium is incorporated as the $AlAlO_3$ fictive component, as shown by the structural formulae in Table 7. The X_{Fe} is within the range 0.3 to 0.5, and calcium, titanium, and manganese contents are always low. The structural formulae calculated on the basis of 4 cations and 6 oxygens, indicate that no Fe^{3+} is present in the melting experiments, but small amounts can be found in crystallisation experiments (Table 7). The average Al_2O_3 contents increase with pressure: 8.0 wt% at 100 MPa, 8.1 wt% at 200 MPa, 9.4 wt% at 300 MPa, where it coexists with cordierite; 9.4 wt% at 500 MPa, 10.4 wt% at 800 MPa, 10.9 wt% at 1 GPa where it coexists with garnet. Alumina is higher in the crystallisation experiments than in the melting experiments. The X_{Fe} decreases slightly with increasing temperature from about 0.5 at 800 °C to less than 0.3 above 1000 °C.

Orthopyroxene is a common product of partial melting of Al-silicate-free rocks such as greywackes, dacites (Conrad et al. 1988), tonalitic gneisses (Skjerlie and Johnston 1992), and S-type granites (Clemens and Wall 1981). However, orthopyroxene compositions have only been published by Conrad et al. (1988). In their experiments with a greywacke, orthopyroxene compositions were similar to those that we obtained, with a high and variable Al_2O_3 content (7–8 wt%). In their experiments with a metaluminous dacite composition, Al_2O_3 contents in orthopyroxene are significantly lower.

Plagioclase (Table 4 and Table 7), a major constituent of the starting material, is present in all the run products, except for two at very high temperatures (A104, 1030–1040 °C). Variations in compositions are of particular interest as it is well known that plagioclase does not reach chemical equilibrium easily (Johannes 1978, 1980).

The MnO (0–0.39 wt%, average 0.09) and TiO_2 (0–0.40 wt%, average 0.11) contents are commonly lower than, or close to, the errors given in Table 1. On the other hand, there are significant amounts of MgO (0.01–0.59 wt%, average 0.16 wt%) and FeO (0.16–1.24 wt%, average 0.45 wt%). For 35 compositions out of 42 the $Al/(K + Na + 2Ca)$ ratio is close to 1, within the limit of the analytical error (6% relative for this ratio, calculated by propagating errors from Table 1). This indicates that the compositions can be interpreted simply in term of albite, orthoclase, and anorthite components. The seven compositions for which there is a marked excess of Al are suspect and will not be considered further. For all compositions, the structural formula calculated on an 8-oxygen basis displays a variable excess of silica, from 0.10 to 0.50 atoms per formula unit, relative to the end-members albite, orthoclase, and anorthite (Table 7). We were unable to find any satisfactory explanation in terms of stoichiometric substitutions to explain this high Si content. We think that it is due to analytical difficulties, the composition of plagioclase being "contaminated" by the surrounding quartz or liquid. Because there is no relationship between the amount of "excess silica" and any other element, it is likely that quartz is the main contaminant. The uncertainty on Si precludes any discussion of the mechanism of incorporation of Fe and Mg because no reliable structural formula can be constructed. For this reason, the plagioclase compositions are given in Table 4 only as albite-orthoclase-anorthite proportions.

Plagioclase compositions from both crystallisation and melting experiments are similar, except for the

Table 2 Biotite compositions. *P* in MPa, *T* in °C; *CEV* biotite composition in the starting material, *P* or *G* for powder or glass, respectively, as starting material; *n* number of analyses used to calculate the average composition, *c* indicate that the analysis has been corrected for "contamination" by the adjacent glass, see text for method; [*X*Fe molar Fe/(Fe + Mg)]

P	*T*	Run no.		*n*	SiO_2	Al_2O_3	FeO	MgO	MnO	CaO	Na_2O	K_2O	TiO_2	Total	*X*Fe
		CEV		7	35.63	19.51	20.62	9.13	0.22	0.00	0.16	9.29	2.80	97.37	0.56
100	803	CE90-2B	P	1	39.28	17.46	14.74	9.27	0.07	0.21	0.92	7.64	2.10	91.69	0.47
	821	CE90-2C	P	1c	42.80	15.21	10.33	13.87	0.88	0.00	0.94	8.02	3.94	95.99	0.29
	854	CE90-2D	P	1	41.88	16.95	7.51	15.98	0.01	0.51	1.23	7.93	2.93	94.93	0.21
200	812	CE89-1B	P	1	41.75	17.89	9.72	13.94	0.14	0.13	0.96	8.70	3.08	96.31	0.28
	825	CE89-1C	P	3	39.84	16.68	9.66	15.29	0.18	0.29	1.19	8.47	3.58	95.18	0.26
300	805	CE90-4A	P	1	41.15	15.54	10.12	15.33	0.16	0.11	0.98	8.46	3.46	95.31	0.27
	810	CE90-3A	P	1	40.07	16.78	12.36	12.51	0.24	0.08	0.88	8.04	3.64	94.60	0.35
	833	CE90-4B	P	1c	40.54	15.84	11.68	13.89	0.12	0.00	0.71	8.67	4.54	95.99	0.32
	834	CE90-3B	G	2	39.83	16.60	12.53	12.41	0.12	0.04	0.93	8.21	4.00	94.67	0.36
	853	CE90-4C	P	1	39.39	16.31	13.25	12.73	0.03	0.06	0.98	8.48	4.02	95.25	0.37
	853	CE90-4C	G	1	39.64	16.02	13.16	13.07	0.03	0.07	0.84	8.32	4.74	95.89	0.36
500	809	A117C	P	5	42.48	17.81	14.18	11.17	0.12	0.20	1.06	8.36	3.59	98.97	0.41
	807	A117C	G	4	39.76	17.50	15.25	12.22	0.16	0.09	0.79	8.81	3.13	97.71	0.41
	851	A99	G	10	37.84	17.27	13.12	13.58	0.13	0.02	0.71	8.68	4.01	95.36	0.35
	867	A117B	P	3	40.40	17.15	13.57	10.94	0.11	0.17	0.86	8.25	4.93	96.38	0.41
	867	A117B	G	6	40.73	15.96	13.13	11.97	0.10	0.09	0.98	8.45	4.37	95.78	0.38
800	855	A109C	P	3	43.55	17.92	14.62	9.64	0.07	0.26	1.30	7.74	3.23	98.33	0.46
	864	A118B	P	1	39.49	16.99	10.80	14.02	0.01	0.12	0.84	9.25	5.12	96.64	0.30
	875	A115C	P	5	39.81	17.43	12.61	13.06	0.04	0.06	0.92	8.73	3.80	96.46	0.35
	879	A109B	P	3	39.63	17.28	14.44	11.60	0.05	0.11	0.92	8.33	4.19	96.55	0.41
	913	A118A	P	2	39.67	17.70	10.59	13.79	0.04	0.27	0.96	8.97	5.02	97.01	0.30
	919	A115B	G	2	38.63	16.90	12.38	13.56	0.05	0.03	0.73	8.92	4.94	96.14	0.34
1000	803	A113C	P	5	41.42	18.49	11.33	11.79	0.12	0.14	0.82	8.53	2.74	95.38	0.35
	858	A113B	P	4	38.59	19.25	11.05	13.10	0.07	0.02	0.78	9.30	3.57	95.73	0.32
	858	A113B	G	4	38.43	18.24	12.17	12.43	0.23	0.05	0.83	9.01	3.03	94.42	0.35
	860	A114C	P	3	39.91	16.93	14.76	11.21	0.06	0.08	0.86	8.99	4.89	97.69	0.42
	874	A113A	P	3	39.44	19.38	10.78	14.25	0.29	0.03	0.66	9.07	3.16	97.06	0.30
	874	A113A	G	3	39.73	17.81	12.95	13.16	0.25	0.04	0.76	9.04	3.58	97.32	0.35
	885	A114B	P	5	38.57	16.46	14.33	12.48	0.03	0.04	0.71	9.03	4.87	96.52	0.39
	885	A114B	G	4	39.32	17.27	15.72	10.36	0.06	0.06	0.54	8.76	4.13	96.22	0.46

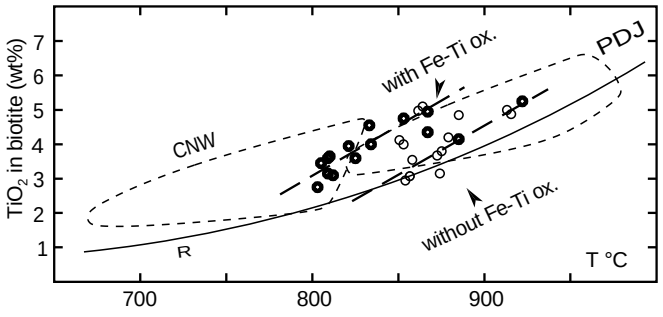

Fig. 1 TiO_2 contents of biotites as a function of temperature. (*Solid circles*: biotite from charges containing an Fe-Ti oxide, *empty circle* biotite from charges without Fe-Ti oxide). *R*, *CNW*, and *PDJ* are labels for the trends obtained by Robert (1976), Conrad et al. (1988) and Patiño-Douce et al. (1993) respectively

orthoclase contents (Or) which are higher in the crystallisation experiments. The Ca/(Ca + Na) is relatively constant between 0.25 and 0.33 (except A114C-G). The orthoclase contents (Or) range from 3.6 mol% to 19.5 mol%, increasing with temperature. At high temperatures, plagioclases are ternary feldspars with Or above 10 mol%. This is consistent with the *solvi* defined by Seck (1971) and Nekvasil (1992), as shown on Fig. 2.

Vielzeuf and Holloway (1988) found a similar An content (An_{21}) with a high Or content (5 mol%), at 875 °C, 1 GPa. Holtz and Johannes (1991) found more calcic compositions, but under fluid-present conditions with higher degrees of melting (Or content was not given). Skjerlie and Johnston (1992) did not provide complete chemical analyses. However, they indicated that the Or contents in plagioclase increased with increasing temperature.

The increasing proportion of Or in plagioclase as a function of temperature is interpreted by Vielzeuf and Montel (1994a) as indicating the production of orthoclase by the melting reaction. It partly explains the absence of alkali feldspar as a discrete phase in the run products, the presence of which has been predicted theoretically (Thompson 1982; Grant 1985; Vielzeuf and Holloway 1988).

Garnet (Table 5) is present at, and above, 500 MPa. The compositions correspond to almandine-pyrope-grossular-spessartine solid solutions, with a small amount of Ti^{4+}. No Fe^{3+} is present following calculations of the structural formula based on 24 oxygens and 16 cations (Table 7). Garnet compositions display significant variations as a function of pressure and temperature. In particular, maximum grossular contents increase with increasing pressure from 4.5 mol% (1.42–1.64 wt% CaO) at 500 MPa, to 6.7 mol% (2.42 wt% CaO) at 800 MPa, and 7.7 mol% (2.77 wt% CaO) at 1 GPa. The increasing proportion of the grossular content can be attributed to the development of the multivariant reaction (II) with increasing pressure. This reaction is characterised by a low dP/dT, and can be used as a geobarometer (Vielzeuf et al. 1991).

Garnet is a common run product in partial melting experiments carried out at medium to high pressures. The compositions obtained by various authors are reported in Fig. 3 for comparison. The main differences with the compositions obtained by other authors are attributed to different bulk compositions (pelites, greywackes, tonalites), and differences in the mineral assemblage coexisting with garnet (Opx-Pl-Qtz in greywackes, Pl-Sillimanite-Qtz in pelites, Cpx-Pl-Qtz in tonalites).

Al-rich spinel (hercynite) was present in the runs only at high temperatures and moderate pressures (300 and 500 MPa). Structural formulae show that it is mainly a $FeAl_2O_4$-$MgAl_2O_4$-Fe_3O_4 solid solution. The compositions reported in Table 6 are only indicative as spinel occurs as very small crystals, and qualitative analyses showed that it contains significant amounts of chromium.

Vielzeuf and Holloway (1988), and Patiño-Douce and Johnston (1991) report the presence of Al-rich spinel in their experiments on pelites at high temperature and at pressures of 700 and 1000 MPa. Compared to the compositions reported by Vielzeuf and Holloway (1988), hercynites from CEV are less aluminous which reflects both a lower Al activity (no Al-silicate) and a higher Fe^{3+} content in our run products. In the pelite experiments, spinel formed according to a reaction involving the breakdown of the aluminium-silicate (Vielzeuf and Holloway 1988). This is not the case in our experiments. Puziewicz and Johannes (1988) obtained hercynite chemically comparable to ours, under water-saturated conditions at NNO oxygen fugacity, and in equilibrium with biotite and cordierite, at 200 and 500 MPa.

Cordierite (Table 6) was found between 100 and 300 MPa. It is magnesium rich (X_{Fe} = 0.20–0.26), and alkali rich (Na_2O = 0.20–0.39 wt%, K_2O = 0.20–0.43 wt%). When the structural formula is calculated on a 18-oxygen basis (Table 7), Si is always higher than 5. This is in contradiction with the mechanism of substitution proposed by Schreyer et al. (1990) Si + · = Al + (Na, K). This suggests that cordierite analyses are contaminated by the surrounding glass or by quartz inclusions (See Fig. 1A in Vielzeuf and Montel, 1994).

Holtz and Johannes (1991) obtained more iron-rich cordierite (X_{Fe} = 0.43–0.33), presumably due to the higher X_{Fe} of their starting material, and lower fO_2 in their experiments (buffered at NNO). Since Fe^{3+} cannot readily be incorporated into cordierite (Deer et al. 1992), high Fe^{3+}/Fe^{2+} increases the $Mg/(Mg + Fe^{2+})$ ratio in the starting material and favours a high Mg content in cordierite. Puziewicz and Johannes (1988) obtained biotite + cordierite together in equilibrium with peraluminous granitic melts at 200 and 500 MPa over the temperature range 710–850°C. As in this study, the cordierites are Na rich (0.35–0.71 wt% Na_2O). However they are generally more iron rich (X_{Fe} around 0.5). Puziewicz and Johannes (1988) showed that X_{Fe} decreases with increasing temperature, and can be as low as 0.21 for 850 °C. This value is very close to that obtained here. Peireira and Bea (1994, Fig. 3), suggested that magmatic

Table 3 Orthopyroxene compositions: *high Al* and *low Al* (third column) are unusual composition coexisting with the average composition. [*XFe* $Fe^{2+}/(Fe^{2+} + Mg)$, *AlPx* 2Al/(2Al + Fe^{2+} + Mg), *En* Mg/(2Al + Fe^{2+} + Mg), *Fs* Fe/(2Al + Fe^{2+} + Mg)]. Other abbreviations as in Table 2

P	*T*	Run no.		*n*	SiO_2	Al_2O_3	FeO	MgO	MnO	CaO	Na_2O	K_2O	TiO_2	Total	*X*Fe	AlPx	Fe	Fs
100	821	CE90-2C	P	1c	48.87	6.72	25.12	17.86	0.66	0.26	0.05	0.00	0.45	99.99	0.44	0.08	0.52	0.41
	854	CE90-2D	P	1	49.21	9.20	18.71	20.87	0.38	0.20	0.18	0.19	0.69	99.63	0.33	0.10	0.60	0.30
200	812	CE89-1B	P	3	48.67	7.79	25.09	17.21	0.63	0.19	0.16	0.17	0.91	100.82	0.45	0.09	0.50	0.41
	825	CE89-1C	P	1	48.67	9.45	21.33	19.44	0.56	0.23	0.19	0.15	0.35	100.37	0.38	0.11	0.56	0.34
	859	CE89-1D	P	2	49.06	7.00	24.86	17.08	0.42	0.29	0.00	0.05	0.55	99.31	0.45	0.08	0.51	0.41
300	810	CE90-3A	P	6	46.48	8.20	28.01	14.27	0.85	0.15	0.07	0.11	0.35	98.49	0.52	0.10	0.43	0.47
	833	CE90-4B	P	5	48.27	9.05	22.20	18.89	0.87	0.20	0.14	0.11	0.39	100.12	0.39	0.10	0.54	0.35
	834	CE90-3B	G	2	43.20	9.52	25.39	15.90	0.79	0.11	0.03	0.06	0.48	95.48	0.44	0.12	0.50	0.39
	853	CE90-4C	P	5	47.38	9.28	24.43	17.39	0.37	0.19	0.09	0.12	0.77	100.02	0.44	0.11	0.50	0.39
	853	CE90-4C	G	5	45.51	9.35	23.85	17.81	0.47	0.13	0.05	0.07	0.31	97.55	0.40	0.11	0.53	0.36
	853	Low Al		1	48.90	5.29	23.11	18.79	0.93	0.20	0.10	0.11	0.30	97.73	0.41	0.06	0.56	0.38
	875	CE90-5	P	1	48.50	8.14	25.89	16.36	0.35	0.25	0.03	0.05	0.73	100.30	0.47	0.09	0.48	0.42
	875		G	8	45.70	10.57	23.51	17.38	0.35	0.13	0.01	0.05	0.48	98.18	0.43	0.12	0.50	0.38
	875	Low Al		1	51.10	4.88	23.27	19.48	0.36	0.15	0.00	0.04	0.34	99.62	0.40	0.06	0.57	0.38
	875	High Al		1	45.74	11.46	24.16	17.36	0.36	0.12	0.03	0.05	0.39	99.67	0.43	0.13	0.50	0.37
500	851	A99	P	1	49.14	10.15	17.40	21.59	0.54	0.15	0.16	0.37	0.21	99.71	0.31	0.11	0.61	0.27
	851	A99	G	7	45.38	10.50	25.84	16.33	0.57	0.13	0.03	0.06	1.01	99.85	0.46	0.12	0.48	0.40
	867	A117B	P	1	48.82	8.37	23.18	18.71	0.43	0.19	0.12	0.11	0.35	100.28	0.41	0.09	0.54	0.37
	867	High Al		1	46.02	13.67	23.75	16.03	0.41	0.15	0.06	0.10	0.42	100.61	0.45	0.16	0.46	0.38
	867	A117B	G	4	46.82	9.60	23.77	18.83	0.49	0.11	0.01	0.04	0.35	100.02	0.39	0.11	0.54	0.35
	867	Low Al		1	53.45	3.89	22.27	22.47	0.67	0.20	0.00	0.00	0.22	103.17	0.36	0.04	0.62	0.34
	883	A97	P	7c	49.18	8.16	20.62	20.70	0.42	0.38	0.09	0.00	0.46	100.01	0.36	0.09	0.59	0.32
	883	A97	G	17	46.92	10.33	23.17	18.16	0.47	0.16	0.02	0.05	0.49	99.77	0.41	0.12	0.52	0.37
	898	A117A	P	11c	47.56	8.78	23.14	18.43	0.42	0.18	0.00	0.00	0.48	98.99	0.41	0.10	0.53	0.37
800	886	A109B	P	2	48.03	8.69	24.62	15.76	0.40	0.27	0.34	0.29	0.30	98.70	0.46	0.10	0.48	0.42
	864	A118B	P	1	53.95	6.82	16.11	24.90	0.35	0.31	0.03	0.41	0.20	103.08	0.26	0.07	0.68	0.25
	875	A115C	P	6	48.61	9.44	23.23	17.41	0.46	0.29	0.06	0.10	0.44	100.04	0.43	0.11	0.51	0.38
	913	A118A	P	1	49.91	12.67	22.64	15.68	0.29	0.26	0.17	0.24	0.63	102.49	0.45	0.15	0.47	0.38
	919	A115B	G	7	48.32	11.06	20.71	19.58	0.50	0.14	0.09	0.10	0.28	100.78	0.37	0.12	0.55	0.33
	942	A115A	P	5	47.43	11.18	21.33	19.34	0.37	0.13	0.12	0.06	0.27	100.23	0.38	0.12	0.55	0.33
	942	A115A	G	6	47.67	10.24	20.21	19.60	0.56	0.24	0.04	0.04	0.42	99.02	0.36	0.12	0.56	0.32
	1026	A104	P	5	48.46	11.19	16.45	22.45	0.40	0.20	0.02	0.01	0.29	99.47	0.29	0.12	0.62	0.25
	1040	A104	G	1	50.34	9.17	16.23	23.03	0.41	0.31	0.10	0.09	0.36	100.04	0.28	0.10	0.65	0.25
1000	860	A114C	G	2	47.84	9.71	29.45	12.27	0.61	0.21	0.27	0.63	0.43	101.42	0.57	0.12	0.38	0.50
	860	A113A	G	1	45.04	12.10	24.58	15.81	1.13	0.27	0.12	0.06	0.38	99.49	0.45	0.14	0.47	0.39
	885	A114B	G	4	47.01	11.44	24.66	15.62	0.61	0.17	0.09	0.02	0.28	99.90	0.47	0.13	0.46	0.41
	922	A120C	P	4	49.04	10.96	24.03	14.41	0.49	0.37	0.27	0.47	0.75	100.79	0.48	0.13	0.45	0.42
	1000	PC92-20	P	7	47.12	10.00	20.50	19.08	0.25	0.27	0.06	0.04	0.53	98.37	0.41	0.12	0.55	0.33
	1000	PC92-20	G	6	46.51	10.98	23.18	18.24	0.34	0.26	0.04	0.07	0.59	100.20	0.38	0.11	0.52	0.37

Table 4 Plagioclase compositions. [*Ab* Na/(Na + K + Ca), *Or* K/(Na + K + Ca), *An* Ca/(Na + K + Ca), molar; F is an alkali feldspar in run A114C]. Other abbreviations as in Table 2; run numbers in italic indicate suspect analyses

P (MPa)			100			200							
T (°C)			821	854		812	825	859					
Run no.	CEVP		CE90-2C	CE90-2D		CE89-1B	*CE89-1C*	CE89-1D					
			P	P		P	P	P					
n			2/6	3/9		2/9	3/8	3/4					
Ab	0.758		0.677	0.683		0.651	0.587	0.643					
Or	0.020		0.052	0.048		0.061	0.086	0.047					
An	0.222		0.271	0.269		0.288	0.327	0.310					
P (MPa)	300												
T (°C)	805	810	833	834	853	853	875	875					
Run no.	CE90-4A	*CE90-3A*	CE90-4B	CE90-3B	CE90-4C	CE90-4C	CE90-5	CE90-5					
	P	P	P	G	P	G	P	G					
n	2/4	2/2	2/7	1/4	1/8	1/4	4/6	1/2					
Ab	0.663	0.696	0.665	0.653	0.631	0.638	0.625	0.585					
Or	0.072	0.043	0.074	0.098	0.076	0.111	0.079	0.071					
An	0.264	0.261	0.261	0.249	0.292	0.252	0.295	0.343					
P (MPa)	500												
T (°C)	809	809	851	851	867	867	883	883	898				
Run no.	A117C	A117C	A99	A99	A117B	*A117B*	A97	A97	A117A				
	P	G	P	G	P	G	P	G	P				
n	1/3	1/2	3/5	4/5	5/10	1/4	9/10	1/8	1/5				
Ab	0.694	0.665	0.585	0.658	0.642	0.605	0.575	0.591	0.634				
Or	0.046	0.060	0.063	0.070	0.086	0.172	0.070	0.114	0.081				
An	0.260	0.275	0.352	0.272	0.272	0.223	0.354	0.295	0.285				
P (MPa)	800												
T (°C)	855	864	975	879	913	919	942	942					
Run no.	A109C	A118B	A115C	A109B	A118A	*A115B*	A115A	*A115A*					
	P	P	P	P	P	G	P	G					
n	3/6	1/1	4/4	3/3	1/4	4/14	5/5	1/2					
Ab	0.693	0.602	0.673	0.693	0.602	0.621	0.598	0.564					
Or	0.041	0.157	0.057	0.036	0.157	0.109	0.173	0.165					
An	0.265	0.241	0.270	0.271	0.241	0.270	0.229	0.271					
P (MPa)	1000												
T (°C)	803	858	858	860	860	860	874	874	885	885	922	1000	1000
Run no.	*A113C*	A113B	A113B	A114C	A114C		A113A	A113A	A114B	*A114B*	A120C	PC92-20	PC92-20
	P	P	G	P	G	F	P	G	P	G	P	P	G
n	1/2	7/8	3/5	5/7	1/3	1/2	4/9	5/8	1/7	1/7	1/3	10/10	5/5
Ab	0.697	0.685	0.696	0.678	0.682	0.381	0.683	0.670	0.654	0.657	0.634	0.595	0.581
Or	0.084	0.062	0.075	0.057	0.152	0.591	0.068	0.074	0.066	0.123	0.111	0.126	0.195
cAn	0.219	0.253	0.229	0.266	0.167	0.027	0.249	0.256	0.280	0.219	0.255	0.279	0.224

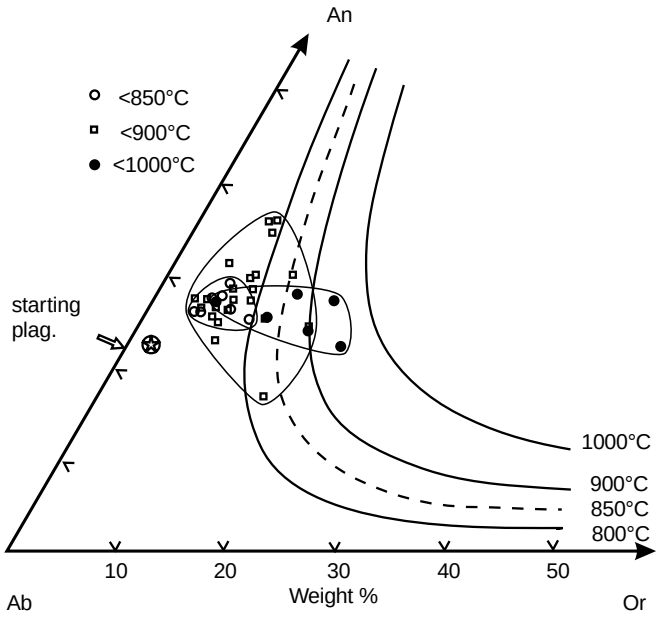

Fig. 2 Projection of plagioclase compositions on the Ab-Or-An plane. The projections of the feldspar solvus at 800, 850 °C, 900 °C, 1000 °C are from Nekvasil (1992) and Seck (1971)

and metamorphic cordierites could be discriminated on the basis of their compositions. In this diagram, our cordierites plot in the magmatic field.

Staurolite (Table 6) was found in only one run (A113C-P), carried-out at 855 °C and 1000 MPa. It has a rather unusual composition with $(Fe^{2+} + Fe^{3+} + Mn)/(Fe^{2+} + Fe^{3+} + Mg + Mn) = 0.61$. This is lower than the normal range (0.69–0.96, Deer et al. 1992).

Gedrite (Table 6) is present in two runs at 800 MPa. However analyses are only available from one (A109-C-P). Conrad et al. (1988) obtained gedrite in greywackes (but not in dacite), close to the solidus, and at low water activities, conditions similar to our experiments. Gedrite compositions here are more aluminous, probably because the $Al^{3+} + Fe^{3+} = Mg^{2+} + Si^{4+}$ substitution is favoured under oxidizing conditions.

Fe-Ti oxides are not present in the starting material. However, they are produced in almost all our runs. Three types of Fe-Ti oxide were recognised: Fe-rich oxides, Fe-Ti oxides, and in some cases, ilmenite. Chemical compositions obtained by the electron probe alone do not allow distinction between ilmenite-hematite and magnetite-ulvospinel solid solutions, except in a few cases where compositions show that the Fe-Ti oxide is undoubtedly ilmenite. The shape of the crystals (small cubes) suggests that the Fe-rich oxides are magnetite.

Glass compositions

Glass compositions are given in Table 8, both uncorrected and corrected (for Na and K). They are silica rich (67–75 wt% SiO_2, average 71.4 wt%), potassic ($1.10 < K_2O/Na_2O < 1.58$ wt%, average 1.33 wt%), and

Table 5 Garnet compositions [*Alm* Fe/(Fe + Mg + Mn + Ca), *Pyr* Mg/(Fe + Mg + Mn + Ca), *Spe* Mn/(Fe + Mg + Mn + Ca), *Grs* Ca/(Fe + Mg + Mn + Ca), molar]. Other abbreviations as in Table 2

P	*T*	Run no.		*n*	SiO_2	Al_2O_3	FeO	MgO	MnO	CaO	Na_2O	K_2O	TiO_2	Total	Alm	Pyr	Spe	Grs
500	809	A117C	P	7	39.74	21.46	26.92	7.61	3.04	1.42	0.03	0.05	0.68	100.95	0.59	0.30	0.068	0.040
	867	A117B	P	2	40.45	21.83	24.18	10.21	1.71	1.64	0.12	0.10	1.09	101.33	0.52	0.40	0.037	0.045
800	855	A109C	P	4	37.67	21.39	27.59	5.78	3.61	1.93	0.09	0.04	0.62	98.72	0.63	0.24	0.083	0.056
	864	A118B	P	2	39.73	22.52	27.07	9.13	0.71	0.48	0.15	0.68	1.58	102.05	0.60	0.37	0.016	0.014
	879	A109B	P	2	38.85	21.65	25.97	8.47	1.15	2.09	0.04	0.04	0.52	98.78	0.58	0.34	0.026	0.060
	875	A115C	P	2	39.34	21.46	23.59	10.36	0.92	2.42	0.08	0.05	1.04	99.26	0.51	0.40	0.020	0.067
	913	A118A	P	6	39.60	22.40	26.66	10.42	0.60	0.75	0.04	0.09	0.50	101.06	0.57	0.40	0.013	0.021
	919	A115B	G	1	39.31	22.48	22.38	12.27	1.32	1.19	0.04	0.02	0.45	99.46	0.47	0.47	0.028	0.032
	942	A115A	P	2	39.50	21.95	22.40	11.32	1.40	1.16	0.01	0.04	0.39	98.17	0.49	0.45	0.031	0.033
1000	858	A113B	P	5	40.67	21.75	21.96	11.10	1.27	2.69	0.08	0.09	0.86	100.47	0.47	0.43	0.028	0.074
	858	A113B	G	1	43.46	29.33	14.46	7.69	4.08	1.02	0.03	0.07	0.26	100.40	0.43	0.41	0.123	0.039
	860	A114C	P	10	39.40	21.75	26.25	8.66	0.87	2.77	0.04	0.04	0.84	100.62	0.57	0.34	0.019	0.077
	874	A113A	P	7	40.52	21.37	18.39	13.87	1.96	2.24	0.11	0.12	0.66	99.24	0.38	0.52	0.041	0.060
	874	A113A	G	1	42.40	22.29	18.71	12.79	4.61	1.30	0.09	0.04	0.28	102.51	0.39	0.48	0.097	0.035
	885	A114B	P	3	39.41	21.44	25.26	9.31	0.54	2.76	0.12	0.06	0.91	99.81	0.55	0.36	0.012	0.077
	885	A114B	G	1	38.90	21.77	26.87	8.53	1.84	2.00	0.03	0.03	0.72	100.69	0.58	0.33	0.040	0.055
	922	A120C	P	3	38.49	21.92	26.56	9.43	0.76	1.16	0.07	0.03	1.19	99.61	0.58	0.37	0.017	0.033
	1000	PC92-20	P	6	39.26	22.35	22.98	12.42	0.56	1.04	0.05	0.04	0.86	99.57	0.49	0.47	0.012	0.028
	1000	PC92-20	G	6	39.64	22.55	25.35	11.37	0.79	1.21	0.08	0.01	1.01	102.0	0.53	0.43	0.017	0.032

Fig. 3 Garnet compositions in a grossular (in mol%)-*X*Fe [Fe/(Fe + Mg) molar] diagram. (*Stars* 500 MPa, *diamonds* 800 MPa, *downward pointing triangles* 1000 MPa; *solid symbols* melting experiments, *empty symbols* crystallisation experiments). Ranges in composition from other experimental studies are reported for a comparison [*PDJ* Patiño-Douce and Johnston (1991), *VH* Vielzeuf and Holloway (1988), *CNW* Conrad et al. (1988), *CW* Caroll and Wyllie (1990)]

peraluminous ($1.12 < \text{A.S.I.} < 1.40$, average 1.23). The CIPW normative compositions are approximately balanced in quartz, albite, and orthoclase components (Fig. 4). The FeO, MgO, and CaO contents are constant and always low (except above 1000 °C) with less than 2 wt% FeO, and less than 1 wt% MgO or CaO. Therefore, all the liquids obtained by partial melting of *CEV* are close to minimum-temperature granitic melt compositions.

The major chemical variations involve the proportions of normative quartz and feldspar and the estimated H_2O contents:

1. In the Q-Ab-Or triangle, the area covered by our compositions is different from the range of water-saturated minimum melt compositions (Tuttle and Bowen 1958; Luth et al. 1964). In all cases, the liquids produced by *CEV*, have higher normative quartz and orthoclase contents than the water-saturated minimum of the same pressure. They have a higher quartz content than the water-undersaturated minimum at the same pressure (Holtz et al. 1992a). Increasing pressure shifts the compositions away from the quartz apex toward the albite-orthoclase side. This fact cannot be interpreted in terms of pressure alone. Temperature, degree of melting, and the water content of the melt are all involved. The respective effects of pressure and water activity, which are well established experimentally, are probably sufficient to explain the main trend. In the haplogranitic system, increasing pressure shifts the minimum toward the albite-orthoclase side (Tuttle and Bowen 1958; Luth et al. 1964; Holtz et al. 1992a), and water undersaturation displaces the minimum toward lower albite/orthoclase (Holtz et al. 1992a).

2. Along the biotite-out curve, the H_2O content of the melt, estimated using phase assemblage mass balance, increases with pressure from 2.5 wt% at 100 MPa to 4 wt% at 1 GPa (Table 8). In our first paper (Vielzeuf

Table 6 Other mineral compositions. [XAl_2O_4] mole fraction of aluminous spinel; *X*Fe = Fe/(Fe + Mg) molar]. Other abbreviations as in Table 2

P	*T*	Run no		*n*	SiO_2	Al_2O_3	FeO	MgO	MnO	CaO	Na_2O	K_2O	TiO_2	Total	
Spinel															XAl_2O_4
300	834	CE90-3B	G	2	5.19	46.95	36.17	8.63	0.51	0.07	0.15	0.23	0.57	98.47	0.91
	853	CE90-4C	G	1	0.89	50.22	37.45	7.70	0.42	0.10	0.00	0.00	0.43	97.21	0.88
	875	CE90-5	G	1	0.71	59.15	30.98	8.61	0.21	0.06	0.00	0.03	0.37	100.12	0.97
500	809	A117C	G	2	0.46	46.39	42.30	6.38	0.65	0.03	0.00	0.07	0.41	96.69	0.82
	867	A117B	P	2	1.78	47.33	42.16	7.17	0.29	0.04	0.00	0.14	0.72	99.63	0.84
	883	A117B	G	1	3.58	49.20	39.86	9.19	0.31	0.15	0.34	0.12	0.58	103.33	0.85
	883	A99	G	1	5.66	50.35	34.12	9.41	0.33	0.11	0.00	0.14	0.54	100.66	0.96
	898	A117A	P	1	0.22	45.46	41.42	6.80	0.27	0.06	0.00	0.01	1.32	95.56	0.81
Cordierite															*X*Fe
100	821	CE92-2C	P	1	51.74	30.29	4.30	9.07	0.04	0.10	0.39	0.43	0.08	96.44	0.21
	854	CE90-2D	P	3	54.56	29.09	4.43	9.90	0.30	0.11	0.29	0.40	0.37	99.44	0.20
200	812	CE89-1B	P	1	49.54	32.79	5.09	10.07	0.15	0.08	0.20	0.20	0.02	98.14	0.22
	825	CE89-1C	P	3	49.39	32.69	5.22	10.10	0.20	0.15	0.30	0.21	0.04	98.30	0.22
	859	CE89-1D	P	7	48.14	32.61	6.03	9.41	0.10	0.15	0.23	0.27	0.06	97.02	0.26
Gedrite															
800	855	A109C	P	4	42.11	17.57	22.11	10.93	0.93	0.49	1.56	0.08	0.53	93.30	0.53
Staurolite															
1000	809	A113C	P	4	27.09	53.91	11.43	4.19	0.35	0.04	0.00	0.03	0.89	97.92	0.52

Table 7 Structural formulae for some selected analyses. The numbers of oxygen for structural formulae is 22 for biotite, 6 for pyroxene, 8 for plagioclase, 24 for garnet, 44 for staurolite, 23 for gedrite, 18 for cordierite, 4 for spinel. The Fe^{3+} content is calculated assuming charge balance and 4 cations in pyroxene, 3 in spinel. Fe^{3+} in staurolite is estimated by filling the Al^{VI}-Ti site to 18

	SiO_2	Al_2O_3	FeO	MgO	MnO	CaO	Na_2O	K_2O	TiO_2	Total	Si	Al^{IV}		Al^{VI}	Fe	Mg	Mn	Ti		K	Na	Ca
Biotite																						
CE89-1B-P	41.75	17.89	9.72	13.94	0.14	0.13	0.96	8.70	3.08	96.31	5.91	2.09		0.89	1.15	2.96	0.017	0.33		1.57	0.26	0.020
A99-G	37.84	17.27	13.12	13.58	0.13	0.02	0.71	8.68	4.01	95.36	5.56	2.44		0.54	1.61	2.99	0.016	0.44		1.63	0.20	0.003
A117B-G	40.73	15.96	13.13	11.97	0.10	0.09	0.98	8.45	4.37	95.78	5.91	2.09		0.64	1.59	2.61	0.012	0.48		1.57	0.28	0.014
A115C-P	39.81	17.43	12.61	13.06	0.04	0.06	0.92	8.73	3.80	96.46	5.73	2.27		0.69	1.51	2.82	0.005	0.41		1.61	0.26	0.009
A109B-P	39.63	17.28	14.44	11.60	0.05	0.11	0.92	8.33	4.19	96.55	5.74	2.26		0.69	1.74	2.52	0.006	0.46		1.54	0.26	0.017
A113B-P	38.59	19.25	11.05	13.10	0.07	0.02	0.78	9.30	3.57	95.73	5.58	2.42		0.86	1.33	2.84	0.009	0.39		1.72	0.22	0.003
A114B-P	38.57	16.46	14.33	12.48	0.03	0.04	0.71	9.03	4.87	96.52	5.63	2.37		0.46	1.74	2.73	0.004	0.53		1.68	0.20	0.006
A114B-G	39.32	17.27	15.72	10.36	0.06	0.06	0.54	8.76	4.13	96.22	5.76	2.24		0.74	1.92	2.28	0.007	0.45		1.64	0.15	0.009
Orthopyroxene											Si	Al^{IV}		Al^{VI}	Fe^{2+}	Fe^{3+}	Mg	Mn	Ca	Na	K	Ti
CE89-1D-P	49.06	7.00	24.86	17.08	0.42	0.29	0.00	0.05	0.55	99.31	1.86	0.14		0.17	0.79	0.000	0.97	0.013	0.012	0.000	0.002	0.016
A97-G	46.92	10.33	23.17	18.16	0.47	0.16	0.02	0.05	0.49	99.77	1.76	0.24		0.22	0.72	0.001	1.02	0.015	0.006	0.001	0.002	0.014
A115C-P	48.61	9.44	23.23	17.41	0.46	0.29	0.06	0.10	0.44	100.04	1.81	0.19		0.23	0.72	0.000	0.97	0.015	0.012	0.004	0.005	0.012
A115A-G	47.67	10.24	20.21	19.60	0.56	0.24	0.04	0.04	0.42	99.02	1.78	0.22		0.22	0.63	0.000	1.10	0.018	0.010	0.003	0.002	0.012
A114B-G	47.01	11.44	24.66	15.62	0.61	0.17	0.09	0.02	0.28	99.90	1.77	0.23		0.28	0.77	0.000	0.88	0.019	0.007	0.007	0.001	0.008
Plagioclase											Si	Al		Na	K	Ca		Fe	Mg	Mn	Ti	
CE89-1D-P	62.00	23.51	0.39	0.09	0.00	5.90	6.78	0.75	0.03	99.45	2.77	1.23		1.59	0.043	0.28		0.014	0.006	0.000	0.001	
CE90-3A-P	62.20	23.46	0.36	0.09	0.01	5.15	7.60	0.71	0.04	99.62	2.77	1.23		0.66	0.040	0.25		0.013	0.006	0.000	0.001	
CE90-5-P	63.57	22.84	0.37	0.07	0.06	5.51	6.46	1.24	0.08	100.20	2.81	1.19		0.55	0.070	0.26		0.014	0.005	0.002	0.003	
A99-G	62.38	23.65	0.50	0.16	0.01	5.31	7.10	1.15	0.08	100.34	2.76	1.23		0.61	0.065	0.25		0.018	0.011	0.000	0.003	
A115C-P	61.37	23.81	0.24	0.07	0.00	5.41	7.46	0.96	0.06	99.38	2.75	1.25		0.65	0.055	0.26		0.009	0.005	0.000	0.002	
A115A-P	62.57	22.46	0.74	0.28	0.09	4.42	6.38	2.80	0.25	99.99	2.80	1.18		0.55	0.160	0.21		0.028	0.019	0.003	0.008	
Garnet											Si		Al	Ti		Fe^{2+}	Mg	Mn	Ca		Na	K
A118A-P	39.60	22.40	26.66	10.42	0.60	0.75	0.04	0.09	0.50	101.06	5.99		3.98	0.06		3.36	2.36	0.08	0.12		0.012	0.017
A114C-P	39.40	21.75	26.25	8.66	0.87	2.77	0.04	0.04	0.84	100.62	6.02		3.91	0.10		3.34	1.98	0.11	0.45		0.012	0.008
Gedrite											Si	Al^{IV}		Al^{VI}	Ti	Mg	Fe	Mn	Ca	Na		Na
A109C-P	42.11	17.57	22.11	10.93	0.93	0.49	1.56	0.08	0.53	96.31	6.31	1.69		1.40	0.06	2.45	2.75	0.12	0.08	0.15		0.31
Staurolite											Si	Al^{IV}		Al^{VI}	Ti	Fe^{3+}		Fe^{2+}	Mg	Mn		
A113C-P	27.09	53.91	11.43	4.19	0.35	0.04	0.00	0.03	0.89	97.93	7.53	0.47		17.13	0.18	0.69		1.96	1.75	0.08		
Cordierite											Si		Al		Fe	Mg	Mn	Ti		K	Na	
CE89-1C	49.39	32.69	5.22	10.10	0.20	0.15	0.30	0.21	*0.04*	98.30	5.03		3.92		0.44	1.54	0.020	0.010		0.030	0.060	
Spinel											Al	Fe^{3+}	Ti	Si		Fe^{2+}	Mg	Mn	Ca		Na	K
CE90-4C-G	0.89	50.22	37.45	7.70	0.42	0.10	0.00	0.00	0.43	97.21	1.76	0.22	0.010	0.027		0.71	0.34	0.011	0.003		0.000	0.000
A117B-P	1.78	47.33	42.16	7.17	0.29	0.04	0.00	0.14	0.72	99.63	1.66	0.27	0.016	0.053		0.77	0.32	0.007	0.001		0.000	0.005

Table 8 Liquid compositions. All iron considered as FeO. Numbers in parentheses for Na_2O and K_2O are the uncorrected values; other abbreviations as in Table 2

P	*T*	Run no		*n*	SiO_2	Al_2O_3	FeO	MnO	MgO	CaO	Na_2O	K_2O		TiO_2		H_2O	Total
100	821	CE90-2C	P	1	72.94	11.99	0.88	0.06	0.37	0.54	2.56	(1.70)	3.58	(3.20)	0.34	2.75	96.01
	854	CE90-2D	P	8	74.36	12.69	1.02	0.05	0.42	0.57	2.61	(1.83)	3.42	(3.11)	0.33	2.31	97.78
200	812	CE89-1B	P	10	74.18	13.35	0.81	0.04	0.28	0.69	2.94	(1.90)	3.57	(3.17)	0.28	2.97	99.11
	825	CE89-1C	P	13	72.00	12.55	0.88	0.07	0.42	0.52	2.96	(1.95)	3.93	(3.51)	0.30	2.82	96.45
	859	CE89-1D	P	13	73.74	12.69	1.33	0.03	0.33	0.91	3.29	(2.24)	3.94	(3.55)	0.34	2.55	99.15
300	805	CE90-4A	P	2	72.47	13.60	0.70	0.05	0.21	0.85	3.54	(2.08)	3.90	(3.35)	0.08	3.81	99.21
	834	CE90-3B	G	4	70.72	12.83	1.29	0.05	0.46	0.45	3.13	(2.71)	4.35	(3.44)	0.28	4.44	98.00
	853	CE90-4C	G	9	70.72	13.26	1.53	0.04	0.53	0.51	3.34	(2.15)	4.51	(4.40)	0.34	4.48	99.26
	875	CE90-5	P	11	71.17	13.93	1.65	0.03	0.37	0.89	3.23	(2.39)	4.19	(4.13)	0.37	2.84	98.67
	875	CE90-5	G	3	72.13	13.54	1.79	0.08	0.89	0.62	2.83	(1.87)	4.25	(3.80)	0.37	2.79	99.29
500	809	A117C	G	7	72.12	13.54	1.37	0.13	0.39	0.66	3.22	(2.71)	4.11	(4.10)	0.16	5.63	101.33
	851	A99	G	5	70.64	14.20	1.46	0.11	0.58	0.59	3.58	(2.01)	4.58	(3.88)	0.21	4.26	100.21
	867	A117B	P	7	74.22	14.32	1.45	0.03	0.37	0.56	3.19	(1.86)	4.53	(3.88)	0.72	3.90	103.29
	867	A117B	G	9	71.55	13.94	1.60	0.06	0.51	0.56	3.60	(3.15)	4.67	(4.61)	0.31	5.13	101.93
	883	A97	P	8	73.32	13.76	1.75	0.04	0.53	0.98	3.29	(2.52)	3.78	(3.73)	0.36	2.45	100.26
	883	A97	G	11	69.56	13.71	1.90	0.05	0.91	0.65	3.26	(2.34)	4.63	(4.55)	0.36	3.17	98.20
	898	A117A	P	9	71.05	13.70	1.71	0.05	0.43	0.65	3.28	(2.96)	4.54	(4.50)	0.33	3.23	98.97
800	875	A115C	P	9	71.00	14.57	1.59	0.05	0.61	0.68	3.47	(2.06)	5.29	(4.56)	0.28	3.73	101.27
	919	A115B	G	6	70.85	14.63	1.45	0.03	0.54	0.65	3.19	(3.19)	5.15	(5.15)	0.25	3.65	100.39
	942	A115A	G	11	70.27	14.02	1.37	0.03	0.67	0.70	3.41	(1.85)	4.89	(4.66)	0.32	4.60	100.28
	1026	A104	P	5	69.80	14.91	2.46	0.10	0.90	1.32	3.50	(2.87)	3.61	(3.58)	0.50	1.76	98.86
	1040	A104	G	8	69.31	14.79	2.28	0.14	0.88	1.59	3.55	(3.35)	3.16	(3.15)	0.37	1.74	97.81
1000	858	A113B	P	5	66.46	14.34	0.84	0.04	0.32	0.58	3.18	(1.98)	3.79	(3.32)	0.18	3.30	93.03
	858	A113B	G	4	69.82	15.37	0.99	0.15	0.39	0.73	3.26	(2.50)	4.61	(4.51)	0.10	8.36	103.78
	874	A113A	G	4	68.44	15.30	1.19	0.10	0.56	0.69	3.29	(3.22)	4.54	(3.87)	0.26	3.73	98.10
	1000	PC92-20	P	8	67.63	15.25	1.82	0.03	0.47	0.76	3.55	(2.39)	5.20	(4.53)	0.37	3.93	99.01
	1000	PC92-20	G	8	69.64	15.47	2.04	0.04	0.59	0.61	3.21	(2.80)	5.67	(5.61)	0.45	4.37	102.09

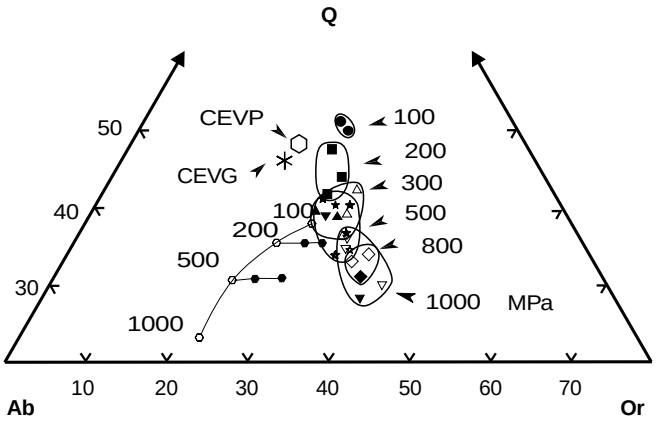

Fig. 4 Central portion of the Q-Ab-Or triangle with the projection of the glass compositions calculated from the CIPW norm. The *small empty hexagons* indicate the position of the water-saturated minima in the haplogranitic system according to Tuttle and Bowen (1958) and Luth et al. (1964) at 100, 200, 500 and 1000 MPa. The *solid hexagons* indicate the positions of the water-undersaturated minima according to Holtz et al. (1992a). *CEVG* and *CEVP* are the projections of the starting materials. (*Circles* 100 MPa, *squares* 200 MPa, *upward triangles* 300 MPa, *stars* 500 MPa, *diamonds* 800 MPa, *downward triangles* 1000 MPa. *Solid symbols* melting experiments, *empty symbols* crystallisation experiments)

and Montel 1994a, Fig. 13), we predicted that the water content of the melt, along the biotite-out curve should lie between 1.7 and 2.2 wt%, using the water solubility model of Nekvasil (Nekvasil and Burnham 1987; Nekvasil 1988). Similar estimates are obtained using the experimental determination of water solubilities in haplogranitic melts published by Holtz and Johannes (1994, Fig. 2). Thus, both models provide estimates lower than the calculated water content of the glasses, that lie commonly above 3 wt%. A possible explanation for this important discrepancy is that minor components (FeO, MgO, CaO) increase the solubility of water in granitic melts, relative to the haplogranitic system. Stern and Wyllie (1981, Fig. 5) suggested that the melt water content at 800 MPa, 930 °C could be as high as 3 wt% based on experimental results from an I-type granite.

Interpretation and discussion

Melt proportions

Melt proportions (Φ in vol.%), as a function of pressure and temperature, are given in Table 9 and Fig. 5. These curves permit a variety of observations:

1. At a given temperature, melt proportion decreases significantly with increasing pressure (e.g. at 850 °C, Φ decreases from 60 to 25 from 100 MPa to 1000 MPa). An important consequence is that the temperature needed to get a large proportion of melt (~40%) increases with pressure. For instance, at 1000 MPa and 1000 °C, Φ is lower than 40.

2. At low pressure (< 500 MPa), the T-Φ curves show an abrupt increase in melt proportion over a limited temperature range (e.g. at 100 MPa, Φ increases from 0 wt% to 73 wt% within a 50 °C interval). With increasing pressure, the T-Φ curves flatten, and the melting intervals increase dramatically (e.g. at 1000 MPa, Φ increases from 20 to 40 within a temperature interval of about 200 °C).

3. At low pressure the onset of melting coincides with the appearance of orthopyroxene. This is no longer true at high pressure where melting begins at a much lower temperature than the Opx-in curve.

This can be interpreted in terms of the solubility of water in the melt and the nature of the reactions involved in the melting process of complex solid solutions such as biotite and plagioclase.

The solubility of water in the silicate melt in the haplogranite system increases with increasing pressure (Tuttle and Bowen 1958; Luth et al. 1964; Holtz and Johannes 1994). Since the amount of water is constant in the system, less melt can be produced at high pressure (Clemens and Vielzeuf 1987). In addition, the fact that higher temperatures are needed to produce a significant proportion of melt at high pressure is in part linked to the fact that the dP/dT slope of the reaction

$$\text{(I)}\ \text{Bt} + \text{Pl} + \text{Qtz} \Longleftrightarrow \text{Opx} + \text{Crd/Grt} + \text{Kfs} + \text{melt}$$

is positive.

Observations (2) and (3) concern the $d\Phi/dT$ relationships and the beginning of melting as a function of pressure. These features result from the fact that reactions other than (I) participate to the breakdown of the assemblage Bt + Pl + Qtz. These are

$$\text{(II)}\ \text{Bt} + \text{Pl} + \text{Qtz} \Longleftrightarrow \text{Grt (alm-pyr-grs)} + \text{Kfs} + \text{melt}$$

and

$$\text{(III)}\ \text{Bt} + \text{Pl} \Longleftrightarrow \text{Grt (alm-pyr-grs)} + \text{Ms}$$

$$(\text{Ms} = \text{muscovite})$$

Both reactions have a negative ΔV, a very small dP/dT slope and correspond to huge multivariant fields in pressure-temperature space. Complex phase relationships involving these reactions are discussed in detail in part I of this study (Vielzeuf and Montel 1994a, Fig. 9). The existence of such reactions, predicted by thermodynamic modelling and demonstrated experimentally, has important implications for the first appearance of melt. Even in experiments carried out with a single composition (here a natural greywacke), the reaction involved in the first appearance of melt may vary with pressure.

For an assemblage of Bt + Pl + Qtz, originally equilibrated at 300 MPa (case 1), as our starting material CEV, the solidus coincides with reaction (I) Bt + Pl + Qtz $\Longleftrightarrow$ Crd/Grt + Opx + Kfs + melt only at P < 300 MPa. In order to understand what happens at higher pressures (e.g. 1000 MPa, 1000 °C), it is necessary to consider a two-step process. During the first isothermal step (e.g. 700 °C), pressure increases from 300 to 1000 MPa. During this stage, biotite and the anorthite component in plagioclase react according to

Table 9 Modal compositions (*Qtz* quartz, *Mag* magnetite, F*e-Ti Ox* Fe-Ti oxide, *Ilm* ilmenite, *St* staurolite, *Ged* gedrite). Melt proportions (vol.%) estimated by mass balance (*M.B.*) or image processing (*I.P.*), with error in parentheses. A *zero* indicates that the phase was present in very small amount but that a small negative proportion was obtained during the mass balance calculation. Other abbreviations as in Tables 1 and 2

P	*T*	Run no.	Mineral proportion in weight%														
			Bt	Pl	Qtz	Mag	Fe–Ti Ox	Ilm	Opx	Hc	Crd	St	Grt	Ged	glass	M.B.	I.P.
100	821	CE90-2C P	9.4	26.5	19.1	3.3	–	–	3.6	–	1.4	–	–	–	38.3	45(5)	40(3)
	854	CE90-2D P	0	22.4	6.7	0.9	2.2	–	11.3	–	0	–	–	–	62.0	69(7)	
200	812	CE89-1B P	11.3	26.6	22.4	3.0	–	–	3.5	–	0	–	–	–	33.0	39(5)	
	825	CE89-1C P	5.6	26.1	17.5	3.1	–	–	6.2	–	0.1	–	–	–	42.8	50(7)	34(3)
	859	CE89-1D P	–	18.3	10.9	1.0	–	1.1	10.6	–	2.6	–	–	–	55.9	63(3)	
300	805	CE90-4A P	14.7	31.4	28.6	3.8	0	–	–	–	–	–	–	–	22.1	27(3)	22(2)
	810	CE90-3A P	13.7	27.3	26.8	2.6	–	–	2.9	–	–	–	–	–	26.7	32(4)	24(3)
	833	CE90-4B P	11.6	31.5	26.7	3.4	–	–	1.2	–	2.8	–	–	–	23.6	28(3)	22(2)
	834	CE90-3B G	10.9	33.6	27.2	2.1	–	–	3.8	1.5	–	–	–	–	22.4	26(4)	
	853	CE90-4C P	7.7	27.0	23.3	2.8	–	0.1	3.4	–	4.8	–	–	–	31.7	38(4)	36(2)
	853	CE90-4C G	9.0	34.8	25.5	1.9	–	–	4.4	1.6	–	–	–	–	23.9	28(3)	
	875	CE90-5 P	–	21.0	14.2	–	–	0.9	13.0	0.2	–	–	–	–	50.3	58(3)	39(3)
	875	CE90-5 G	–	22.2	13.6	–	–	1.0	11.2	0.1	–	–	–	–	51.3	58(6)	
500	809	A117C P	17.5	28.3	31.5	2.2	–	–	–	–	–	–	1.6	–	17.7	22(3)	17(6)
	809	A117C G	18.0	33.2	32.5	1.5	–	–	–	1.3	–	–	–	–	12.9	15(3)	
	851	A99 G	12.3	29.3	30.5	2.7	0	–	2.9	–	–	–	–	–	22.0	27(4)	
	867	A117B P	9.8	28.3	25.4	2.2	–	–	6.0	0	–	–	0	–	26.6	32(3)	39(2)
	867	A117B G	11.0	34.5	28.6	1.8	–	–	2.0	2.4	–	–	–	–	19.3	23(2)	
	883	A97 G–		19.7	22.0	–	1.9	–	9.5	–	–	–	–	–	45.1	53(3)	
	883	A97 P	–	16.8	11.5	1.2	1.3	–	10.5	–	–	–	–	–	58.3	66(3)	63(2)
	898	A117A P	–	23.3	18.6	0.5	1.3	–	10.9	1.1	–	–	–	–	44.3	51(3)	49(2)
800	855	A109C P	22.1	30.5	31.3	1.6	0	–	–	–	–	–	0.4	1.2	12.4	16(4)	10(3)
	875	A115C P	4.1	23.4	24.9	0	1.7	–	5.9	–	–	–	5.4	–	33.9	40(5)	23(5)
	879	A109B P	6.4	26.1	24.8	–	1.3	–	7.7	–	–	–	2.3	–	30.6	36(4)	23(3)
	913	A118A P	4.2	28.8	25.0	1.3	–	0.7	7.9	–	–	–	3.0	–	28.5	34(7)	32(2)
	919	A115B G	0	27.9	21.5	–	2.4	–	11.0	–	–	–	0.2	–	36.3	43(4)	
	942	A115A P	–	26.3	21.6	–	2.1	–	7.2	–	–	–	2.8	–	40.0	47(5)	36(7)
	942	A115A G	–	32.1	22.8	–	2.6	–	11.0	–	–	–	–	–	31.1	37(6)	
	1026	A104 P	–	–	9.7	–	2.1	–	7.1	–	–	–	–	–	81.3	87(5)	85(3)
	1040	A104 G	–	–	9.3	–	2.5	–	7.0	–	–	–	–	–	82.4	88(3)	
1000	803	A113C P	18.8	30.3	33.6	3.1	0	–	–	–	–	1.0	–	–	14.3	18(2)	15(3)
	858	A113B P	10.4	22.5	27.2	–	1.1	–	–	–	–	–	9.7	–	30.7	37(7)	13(4)
	858	A113B G	17.5	34.5	35.0	–	2.8	–	–	–	–	–	1.7	–	8.7	11(6)	
	860	A114C P	12.5	24.7	30.1	–	0.1	–	–	–	–	–	9.0	–	22.9	28(6)	26(3)
	874	A113A P	9.4	29.4	28.8	–	3.0	–	–	–	–	–	6.0	–	23.4	29(8)	23(3)
	874	A113A G	8.4	26.7	27.4	–	1.1	–	7.8	–	–	–	0	–	21.3	26(2)	
	885	A114B P	9.8	24.9	28.0	–	0.4	–	–	–	–	–	10.3	–	26.0	32(5)	24(2)
	885	A114B G	14.3	32.0	29.6	1.7	–	–	5.1	–	–	–	0	–	17.1	21(3)	
	1000	PC92-20 P	–	24.0	25.0	–	2.1	–	7.9	–	–	–	5.1	–	36.0	43(2)	
	1000	PC92–20 G	–	27.0	25.0	–	1.7	–	10.0	–	–	–	2.8	–	33.0	39(3)	

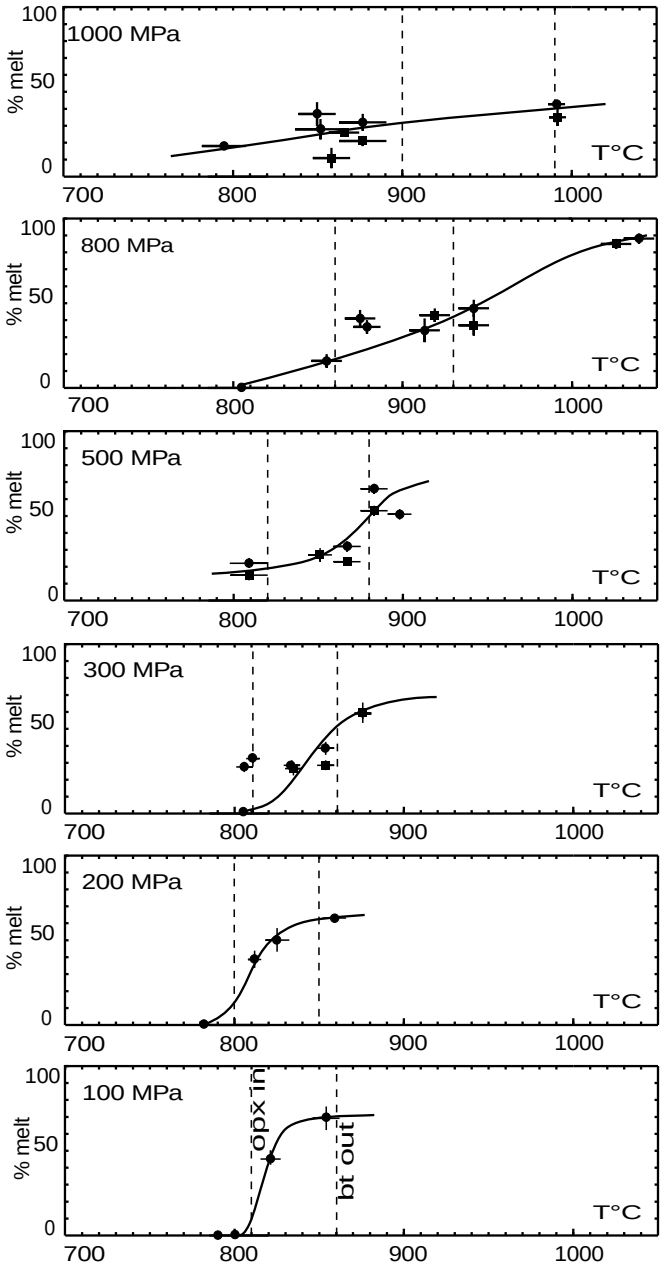

Fig. 5 Proportion of melt as a function of temperature at different pressures. (*Circles* melting experiments, *squares* crystallisation experiments). The *lines* correspond to visual fits

reaction (III) to give garnet and muscovite (Ms). This results in the development of the assemblage Bt_{II} + - Pl_{II} + Qtz + Grt(alm-pyr-grs) + Ms. There is no obligation for biotite or plagioclase to disappear entirely during the pressure increase because reaction (III) corresponds to a very wide multivariant field. The second step is an increase in temperature (e.g. from 700 to 1000 °C) at constant pressure (1000 MPa). Because of the presence of newly formed muscovite, the first melt will be produced by reaction

(IV) Ms + Pl + Qtz $\Longleftrightarrow$ Bt + Als + Kfs + melt

(Als = Aluminium silicate) at about 800 °C. Biotite fluid-absent melting will take place at a higher temperature (ca 890–990°C) according to reaction (I) Bt + Pl + Qtz $\Longleftrightarrow$ Grt + Opx + Kfs + melt. Thus, at high pressures, the beginning of melting does not coincide with the appearance of orthopyroxene but rather with the breakdown of muscovite. This conclusion is valid, at least up to 2000 MPa, for the fluid-absent melting of most pelites and aluminous greywackes since muscovite is a common phase in both rock types in the subsolidus at high pressure.

Interestingly, at 1000 MPa, a rock strictly composed of an assemblage of Bt + Pl + Qtz (no muscovite) in thermodynamic equilibrium in the subsolidus at 700 °C (case 2) would start melting through reaction (I), thus at a higher temperature than in case 1.

From the experimental data collected at each pressure, the positions of the "isotects" (curves that join identical degree of melting) can be determined. This allows the construction of a P-T-Φ diagram (Fig. 6). At low pressures, the negative slope of the isotects is most probably due to the negative slope of reaction (I) over this pressure interval (Vielzeuf and Montel 1994a, Fig. 2). Between 200 to 700 MPa, all the isotects have positive dP/dT slopes. Above 700 MPa, the slopes of some isotects change. For instance the Φ = 20 curve moves toward lower temperatures probably because reactions (III) and (IV) now play increasing roles as pressure increases. In contrast, the other isotects are displaced toward higher temperatures related to the slope of reaction (I).

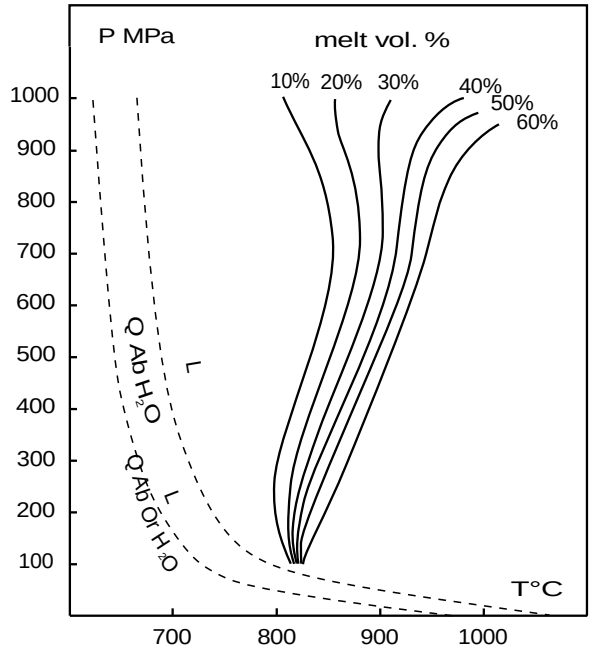

Fig. 6 Pressure-temperature projections of some isotects as estimated from Fig. 5. The Q-Ab-Or-H_2O and Q-Ab-H_2O *solidi* are reported for reference

In summary, the funnel shape of the isotects can be explained by the dP/dT slopes of the melting reactions and the interferences between complex reactions (I), (II), (III), (IV).

The melt proportions that we measured are lower than what we predicted from water solubility models (Vielzeuf and Montel 1994a). For example at 800 MPa, 930 °C, along the biotite-out curve, the predicted water content was 2–2.2 wt%, which should correspond to 65–72 wt% melt (72–78 vol.%). This is not compatible with the 45 vol.% estimated by mass balance and image processing in the four charges that bracket the biotite-out curve at this pressure. A possible explanation is that the available solubility models based on data in the haplogranitic system may not adequately predict the water contents of the melts in a more complex system.

Proportions of crystals

At low pressure, the modal proportions of quartz and biotite show a rapid decrease with increasing temperature, whereas the plagioclase content decreases slowly (Table 9). At the same time orthopyroxene and cordierite contents increase. At higher pressure, biotite, quartz and plagioclase abundances decrease slowly with increasing temperature. The orthopyroxene contents increase with temperature. However the results from runs at 800 MPa, 1026 and 1040 °C suggest that orthopyroxene started dissolving into the melt. The modal proportion of garnet plotted against temperature always displays a bell-shaped curve at all pressures.

The runs that correspond to the multivariant field defined by the assemblage Opx + Bt + Pl + Grt + Qtz + melt confirm the predictions made by Vielzeuf and Montel (1994a, Table 4) on the basis of geometrical phase relationships. However the new data provide additional information. With increasing pressure at a given temperature, reaction (II) should consume biotite, plagioclase and quartz. However, at the same time, these minerals should be produced by reaction (I) because of its positive slope. The observed modal abundances indicate that up to 1 GPa, reaction (I) dominates. Thus the overall effect of increasing pressure at a fixed temperature and within the previously defined P-T interval, is to increase the modal content of biotite, plagioclase, and quartz. The involvement of reaction (II) can be detected through increasing grossular content in garnet, and the backbending of the 20% isotect. Variations in plagioclase modal proportions are more difficult to predict, because the orthoclase, albite, and anorthite components behave independently from one another. From the observed modal proportions in the runs, it seems that the various feldspar-consuming and feldspar-producing reactions balance each other. Thus the overall plagioclase content remains close to the initial mode within the previously defined P-T surface. Although plagioclase is involved in all the important reactions in the system, its modal proportion is a complex function of the variations of the three main components. This applies for most other solid solutions and emphasises the importance of resolving the solid solutions into their respective end-members for petrological discussion.

Melt productivity of some crustal rock types

Compared to other lithologies, the greywacke investigated in this study has an intermediate fertility. Although the beginning of melting coincides for pelites and greywackes as both involve the breakdown of muscovite (Vielzeuf and Montel 1994b), extensive melting of pelites occurs at a significantly lower temperature than greywackes. According to the experiments of Patiño-Douce and Johnston (1991), the 20 vol.% isotect for pelites is about 40 °C lower than that of greywackes at 700 MPa. The composition of the pelite investigated by Vielzeuf and Holloway (1988) was found to be more fertile: at 875 °C, 1 GPa, 50 vol.% melt was produced, whereas Patiño-Douce and Johnston (1991) obtained only 35 vol.%. Under the same pressure-temperature conditions, the partial melting of our greywacke produces 25 vol.%. The difference in melting behaviour between the two pelites can be explained in terms of their chemical composition: the pelite used by Patiño-Douce and Johnston (1991) is poor in Na_2O, and SiO_2, thus poor in quartz and albite components. In terms of stoichiometric coefficients for the peritectic reaction, the relative proportion of phases within the starting material used by Vielzeuf and Holloway (1988) was found to be closer to the ideal mixture required to get the maximum amount of melt.

The difference in fertility between pelites and greywackes can be attributed to the nature of the melting reaction involved and their stoichiometric coefficients. The biotite breakdown reaction for pelites involves aluminium-silicate:

$$\text{(V)}\quad \text{Bt} + \text{Pl} + \text{Als} + \text{Qtz} \Longleftrightarrow \text{Grt} + \text{Kfs} + \text{Ilm} + \text{melt}$$

This reaction occurs at a temperature lower than that of reaction (I) (Vielzeuf and Holloway 1988; Le Breton and Thompson 1988, Patiño-Douce and Johnston 1991). This is in agreement with the fact that excess Al_2O_3 (normative corundum) in granitic melts lowers the temperature of the minima in synthetic granitic systems (Holtz et al. 1992b; Joyce and Vogt 1994). The difference in fertility between pelites and greywackes is greater at high pressure, because reaction (I) has a significant dP/dT slope, whereas reaction (V) is almost isothermal in the 600–1200 MPa range (Vielzeuf and Holloway 1988). Thus, greywackes are less fertile than pelites at high pressure (above 700 MPa). However, at moderate pressure (300–700 MPa) both rock types are more or less equally fertile because the difference in temperature between the Al-silicate-free and Al-silicate-present biotite breakdown reactions is smaller. Furthermore, the melting reactions for pelites and greywackes converge toward 600 MPa and 850 °C. Here, partial melting of both

lithologies almost coincides making this pressure-temperature domain particularly important for granitoid magma genesis (Vielzeuf and Montel 1994b).

Other rock types make less fertile sources for granitic magmas. For instance, tonalites produce only 10 vol.% melt at 1000 MPa, 875 °C (Rutter and Wyllie 1988) or 950 °C (Skjerlie and Johnston 1992). The low fertility of tonalites can be explained by the high calcium content of the plagioclase. Since calcium is preferentially incorporated into the plagioclase rather than the melt, it can be predicted that Bt-Pl-Qtz rocks with calcic plagioclase will be less fertile than *CEV*. Amphibolites are not very fertile either. Rapp et al. (1991) located the 10 vol.% isotect at 950 °C and 1 GPa. For the most fertile composition they investigated, Beard and Lofgren (1991) found the 10 vol.% isotect at 875 °C, and the 20 vol.% isotect at 950 °C (690 MPa in each case). The low fertility of amphibolites can be explained by the facts that they are rich in calcium, that amphibole melting reactions occur at higher temperatures than those involving biotite, and that they are poor in quartzo-feldspathic components.

Experimental partial melts and the origin of crustal granites

The compositions of the melts obtained experimentally by several authors have been projected onto the Q-Ab-Or triangle in Fig. 7. Most of the melts have normative quartz contents of 30 to 50 wt%. This corresponds to the approximate quartz/feldspar (alkali feldspar + plagioclase) ratio in the haplogranite minima. Also the K/Na ratio in the liquid can be directly related to the K/Na ratio in the starting material. Patiño-Douce and Johnston (1991) obtained the most potassic melts with a K-rich, Na-poor pelite (K_2O/Na_2O = 7.6); Conrad et al. (1988) obtained sodic melts with an immature, sodic greywacke (K_2O/Na_2O = 0.5), and a dacite (K_2O/Na_2O = 0.5). Vielzeuf and Holloway (1988), Holtz and Johannes (1991) and Montel and Vielzeuf (this work), starting from balanced compositions (K_2O/Na_2O = 1.5, 1.3, 0.8 respectively) obtained liquids with intermediate K/Na ratios. Partial melting of amphibolites (Rapp et al. 1991; Beard and Lofgren 1991; Rushmer 1991), produces sodic liquids (tonalite, trondhjemite), which are definitely not granitic in composition. Thus, as far as the Q-Ab-Or proportions are concerned, it is clear that not all crustal sources are able to produce melts of granitic composition. Only those with K/Na ratio close to unity will produce truly granitic compositions in significant amounts.

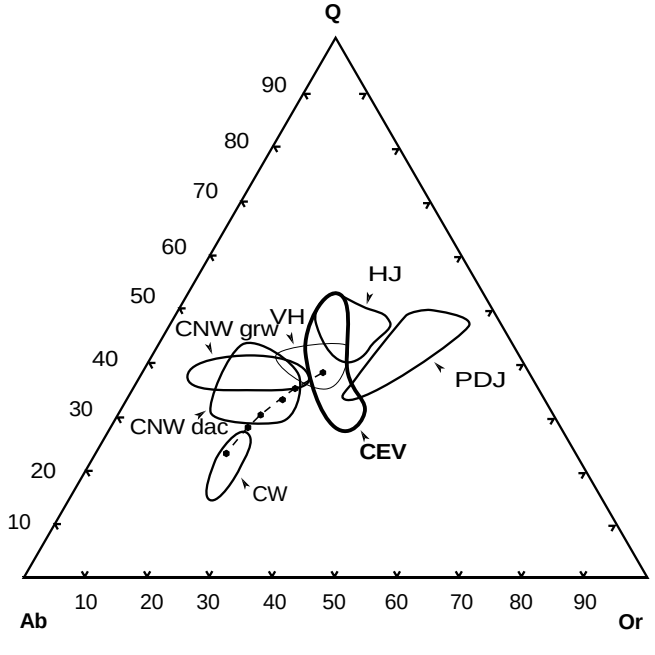

Fig. 7 Compositions of experimental glasses from available experimental studies projected on the Q-Ab-Or plane (CIPW norm). [*HJ* Holtz and Johannes (1991), *PDJ* Patiño-Douce and Johnston (1991), *VH* Vielzeuf and Holloway (1988), *CNWgrw* and *CNWdac* Conrad et al. (1988) from greywackes and dacite respectively, *CW* Caroll and Wyllie (1990), *CEV* this study]. The positions of the water-saturated minima (*hexagons*) are also shown

The compositions of some typical granitic suites are compared to the experimental glasses obtained in this study (Table 10). Melts formed at 500 MPa, or above, have compositions similar to those of peraluminous leucogranites. Felsic end-members of S-type granite series are similar to the melts formed at low pressure (300 MPa or less).

The compositions of published experimental melt compositions together with those of some representative granitic suites are reported in Fig. 8. In this diagram, excess alumina (A) is plotted against Fe + Mg + Ti (B) following a method proposed by Debon and Le Fort (1982). Feldspars and quartz plot at the origin, and thus it is the quartzo-feldspathic part of the composition that is emphasized. All the partial melts produced by our starting material (*CEV*) plot in the field of leucogranite suites (CARN, HH, GG in Fig. 8) with a vertical trend similar to the one defined by the High Himalayas leucogranites (Debon and Le Fort 1982). Melt compositions obtained from pelites (Patiño-Douce and Johnston 1991) and from greywackes (Conrad et al. 1988) are also peraluminous and felsic (Fig. 8). However, they have different K_2O/Na_2O ratios (Fig. 7). Partial melting of peraluminous granitoids (Holtz and Johannes 1991; Clemens and Wall 1981) produced strongly peraluminous and felsic melts also. Metaluminous source rocks such as dacite or tonalite (Conrad et al. 1988; Caroll and Wyllie 1990) produced metaluminous or weakly peraluminous melts.

Interestingly, some common granite compositions have not yet been produced by direct experimental anatexis of any source rock, despite the wide range of starting materials investigated so far. For instance, no partial melt that would replicate the mafic end-members present in most granitic suites (FeO = 3–6 wt%, MgO = 1.5–3.5 wt%, CaO = 1.9–6 wt%), either peraluminous or metaluminous, has ever been obtained.

Table 10 Comparison between granites and experimental glasses. Analyses normalized to 100% anhydrous, with all Fe recalculated to FeO. Corsica: Ile Rousse magnesio-potassic sub-alkaline series (Laporte et al. 1991); post-anatectic peraluminous cordierite-bearing granites Massif Central (Montel and Abdelghaffar 1993); Moruya: Australian I-type series (Chappell and Stephens 1988); Peninsular Ranges Batholith, average composition (Silver and Chappell 1988); Bullenbalong and Strathbogie: Australian S-type series (White and Chappell 1988); Granodiorite and Leucogranites average composition from the French Massif Central (Didier and Lameyre 1969); Gangotri: average composition of the Badrinath-Gangotri leucogranite, high Himalayas (Scaillet et al. 1990); Manaslu: leucogranite, average composition, High Himalayas (Vidal et al. 1982); Carnmenellis: leucogranite, typical composition, Cornubian Batholith (Charoy 1986)

P	*T*		SiO_2	Al_2O_3	FeO	MnO	MgO	CaO	Na_2O	K_2O	TiO_2
			Glasses								
100	821	P	78.21	12.86	0.94	0.06	0.40	0.58	2.75	3.84	0.36
	854	P	77.89	13.29	1.07	0.05	0.44	0.60	2.73	3.58	0.35
200	812	P	77.16	13.89	0.84	0.04	0.29	0.72	3.06	3.71	0.29
	825	P	76.90	13.40	0.94	0.07	0.45	0.56	3.16	4.20	0.32
	859	P	76.34	13.14	1.38	0.03	0.34	0.94	3.41	4.08	0.35
300	805	P	75.96	14.26	0.73	0.05	0.22	0.89	3.71	4.09	0.08
	834	G	75.59	13.71	1.38	0.05	0.49	0.48	3.35	4.65	0.30
	853	G	74.61	13.99	1.61	0.04	0.56	0.54	3.52	4.76	0.36
	875	P	74.27	14.54	1.72	0.03	0.39	0.93	3.37	4.37	0.39
	875	G	74.75	14.03	1.85	0.08	0.92	0.64	2.93	4.40	0.38
500	809	G	75.36	14.15	1.43	0.14	0.41	0.69	3.36	4.29	0.17
	851	G	73.62	14.80	1.52	0.11	0.60	0.61	3.73	4.77	0.22
	867	P	74.68	14.41	1.46	0.03	0.37	0.56	3.21	4.56	0.72
	867	G	73.92	14.40	1.65	0.06	0.53	0.58	3.72	4.82	0.32
	883	P	74.96	14.07	1.79	0.04	0.54	1.00	3.36	3.86	0.37
	883	G	73.20	14.43	2.00	0.05	0.96	0.68	3.43	4.87	0.38
	898	P	74.21	14.31	1.79	0.05	0.45	0.68	3.43	4.74	0.34
800	875	P	72.79	14.94	1.63	0.05	0.63	0.70	3.56	5.42	0.29
	919	G	73.24	15.12	1.50	0.03	0.56	0.67	3.30	5.32	0.26
	942	G	73.44	14.65	1.43	0.03	0.70	0.73	3.56	5.11	0.33
1000	858	P	74.07	15.98	0.94	0.04	0.36	0.65	3.54	4.22	0.20
	858	G	73.17	16.11	1.04	0.16	0.41	0.77	3.42	4.83	0.10
	874	G	72.52	16.21	1.26	0.11	0.59	0.73	3.49	4.81	0.28
	1000	P	71.13	16.04	1.91	0.03	0.49	0.80	3.73	5.47	0.39
	1000	G	71.26	15.83	2.09	0.04	0.60	0.62	3.28	5.80	0.46
					Granites						
Corsica			62.46	17.34	4.70	0.07	2.97	3.75	3.63	4.12	0.96
			69.92	15.09	2.66	0.06	1.45	2.26	3.30	4.73	0.52
Post anatectic granites (Velay)			66.95	15.50	5.05	0.06	1.60	2.07	3.26	4.50	1.01
			73.39	14.13	1.70	0.03	0.51	0.88	3.31	5.77	0.27
Moruya (I-type)			62.10	16.96	5.63	0.11	3.34	6.04	4.18	1.45	0.19
			75.96	14.17	0.48	0.07	0.24	1.12	4.27	3.55	0.15
Peninsular Range Batholith			65.69	12.20	4.34	0.08	2.18	5.18	3.68	1.98	0.66
Bullenballong (S-type)			67.34	15.35	5.37	0.07	2.64	2.96	2.05	3.53	0.69
			74.94	13.61	1.98	0.05	0.76	1.28	2.65	4.60	0.12
Strathbogie (S-type)			72.01	14.44	3.60	0.06	1.16	1.88	2.63	4.04	0.18
			77.14	13.01	1.04	0.05	0.16	0.55	3.05	4.87	0.13
Granodiorite (Massif Central)			68.37	15.80	3.79	0.05	1.83	2.09	3.38	4.28	0.41
Leucogranites (Massif Central)			73.91	14.83	1.52	0.00	0.95	0.81	3.36	4.45	0.17
Gangotri (Himalayas)			68.37	15.80	3.79	0.05	1.83	2.09	3.38	4.28	0.41
Manaslu (Himalayas)			73.91	14.83	1.52	0.00	0.95	0.81	3.36	4.45	0.17
Camenellis (Cornubian batholith.)			73.55	15.12	1.57	0.04	0.29	0.71	3.17	5.29	0.25

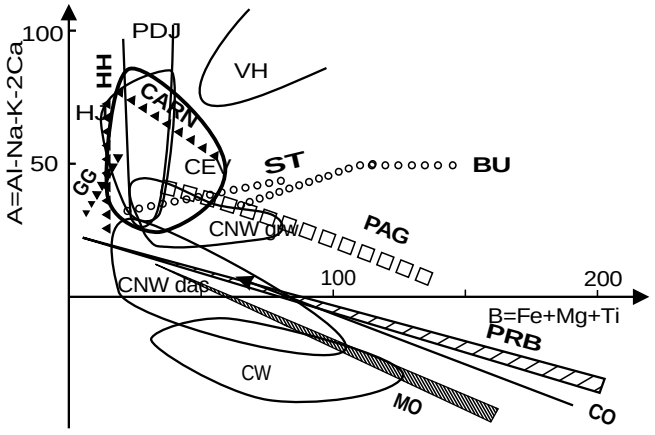

Fig. 8 Compositions of experimentally derived melts in the A-B diagram of Debon and Lefort (1982) [*HJ* Holtz and Johannes (1991), *PDJ* Patiño-Douce and Johnston (1991), *VH* Vielzeuf and Holloway (1988), *CNWgrw* and *CNWdac* Conrad et al. (1988) from greywackes and dacite respectively, *CW* Caroll and Wyllie 1990, *CEV* (*thick line*) this study]. Various reference natural series are reported for comparison [*HH* High Hymalayas (Vidal et al. 1982), *GG* Gangotri (Scaillet et al. 1990), *CARN* Carnmenellis pluton, Cornubian batholith (Charoy 1986), *CO* Ile-Rousse, Corsica (Laporte et al. 1991), *PAG* post-anatectic peraluminous series, French Massif Central (Montel and Abdelghaffar 1993), *MO* Moruya (Chappell and Stephens 1988), *PRB* Peninsular Ranges Batholith (Silver and Chappell 1988), *BU* and *ST* Bullenbalong and Strathbogie (White and Chappell 1988)]

This suggests that such natural compositions do not represent pure anatectic crustal melts but involve other components such as restite or cumulative minerals or mafic mantle-derived liquids.

Conclusion: metagreywackes as a source for granites

Metagreywackes similar to *CEV* are fertile at moderate pressure (300–700 MPa) and produce 30 to 60 vol.% melt at about 900 °C by fluid-absent melting of biotite. Above 800 MPa, they are less fertile than pelites as the main melting reaction producing orthopyroxene has a positive dP/dT slope. However, they are always more fertile than amphibolites or tonalites. At high pressure, the beginning of melting of greywackes does not coincide with the appearance of orthopyroxene. This is because there are other reactions that may produce up to 20 vol.% melt, 100 °C lower than the Opx-in boundary.

The liquids produced from partial melting of metagreywackes are leucocratic and peraluminous over the whole pressure-temperature range investigated, even for degrees of melting as high as 60 vol.%. These melt compositions are similar to leucogranites, such as those from the High Himalayas, the Massif Central or the Cornubian Batholith. Since other protoliths (pelites, orthogneisses) also produce leucogranitic melts by partial melting, we can infer that the generation of more mafic granitoids requires a combination of processes coeval or subsequent to simple crustal anatexis. In the case of mafic peraluminous granites such as Australian S-types, restite unmixing is one of such mechanisms. For the generation of widespread metaluminous calc-alkaline or sub-alkaline batholiths such as the Coastal Batholith in Peru, the Corsican Batholith, the Massif Central granodiorites, or the Sierra Nevada Batholith, interactions between mafic mantle-derived melts and anatectic melts are likely. The interaction processes may involve simple mixing, assimilation and fractional crystallisation, or more complex interactions involving simultaneous melting and crystallisation (Huppert and Sparks 1988). The abundance of this type of granite throughout the world, relative to the small volume of peraluminous leucogranites, indicates that such complex interactions between different chemical reservoirs coupled with a wide variety of processes represent the most common way of generating granites. It must be stressed that experimental petrology only provides constraints on the nature of the liquids produced during partial melting. However most granites are not simple partial melts. Rather they are complex solid-liquid suspensions that have been subjected to a variety of physical and chemical processes and interactions during their ascent through the crust, from their source region to their final level of emplacement.

Acknowledgements This study has been supported by CNRS-INSU through contracts 91 DBT 3.28, 91 DBT 4.09, and project "Protocroûte Continentale" action spécifique INSU, 1993. Some experiments and analyses were performed in collaboration with R. Kryza and E. Moinet. They are gratefully acknowledged for their help. This work benefited from microprobe and SEM technical assistance from M. Veschambre and A.M. Mafille. We extend our thanks to J. Bouloton, A. Provost and D. Laporte who helped us clarify our views and interpretations. M. Roberts and P. King carefully reviewed the last version of the manuscript and suggested constructive revisions. Thorough reviews by F. Bea and D.B. Clarke, as well as the scientific comments and the careful editorial work by W. Schreyer were also greatly appreciated. This is contribution CNRS-INSU-DBT no. 64, Thème "Fluides, Minéraux et Cinétique".

References

Albarède F, Provost A (1977) Petrological and geochemical mass-balance equation: an algorithm for least-square fitting and general error analysis. Comput Geosci 3: 309–326

Ancey M, Bastenaire F, Tixier R (1978) Application des méthodes statistiques en microanalyse. In: Maurice F, Meny L, Tixier R (eds) Microanalyse, microscopie électronique à balayage. Les Editions du Physicien, Orsay, France, pp 323–347

Beard JS, Lofgren GE (1991) Dehydration melting and water-saturated melting of basaltic and andesitic greenstones and amphibolites at 1, 3, 6.9 kbar. J Petrol 32: 365–401

Burnham CW (1979) The importance of volatile constituants. In: Yoder HSJr (ed) The evolution of the igneous rocks. Princeton University Press, Princeton, USA, pp 439–482

Burnham CW, Nekvasil H (1986) Equilibrium properties of granite pegmatite magmas. Am Mineral 71: 239–263

Caroll MR, Wyllie PJ (1990) The system tonalite-H_2O at 15 kbar and the genesis of calc-alkaline magmas. Am Mineral 75: 345–357

Castaing R (1960) Advances in electronics and electron physics, vol 13. Academic Press, New York

Chappell BW, Stephens WE (1988) Origin of infracrustal (I-type) granite magmas. Trans R Soc Edinburgh Earth Sci 79: 71–86

Charoy B (1986) The genesis of the Cornubian batholith (South-West England): the example of the Carnmenellis pluton. J Petrol 27: 571–604

Clemens JD (1984) Water contents of silicic to intermediate magmas. Lithos 17: 273–287

Clemens JD, Vielzeuf D (1987) Constraints on melting and magma production in the crust. Earth Planet Sci Lett 86: 287–306

Clemens JD, Wall VJ (1981) Origin and crystallization of some peraluminous (S-Type) granitic magmas. Can Mineral 19: 111–131

Conrad WK, Nicholls IA, Wall VJ (1988) Water-saturated and -undersaturated melting of metaluminous and peraluminous crustal compositions at 10 kbar: evidence for the origin of silicic magmas in the Taupo volcanic zone, New Zealand, and other occurences. J Petrol 29: 765–803

Debon F, Le Fort P (1982) A chemical-mineralogical classification of common plutonic rocks and associations. Trans R Soc Edinburgh Earth Sci 73: 135–149

Deer WA, Howie RA, Zussman J (1992) An introduction to the rock-forming minerals. Longman, London

Didier J, Lameyre J (1969) Les granites du Massif Central français: étude comparée des leucogranites et granodiorites. Contrib Mineral Petrol 24: 219–238

Grant JA (1985) Phase equilibria and partial melting of pelitic rocks. In: Ashworth JR (ed) Migmatites. Blackie and Sons, Glasgow, pp 86–144

Holtz F, Johannes W (1991) Genesis of peraluminous granites I. Experimental investigation of melt compositions at 3 and 5 kbar and various H_2O activities. J Petrol 32: 935–957

Holtz F, Johannes W (1994) Maximum and minimum water contents of granitic melts, implications for chemical and physical properties of ascending magmas. Lithos 32: 149–159

Holtz F, Pichavant M, Barbey P, Johannes W (1992a) Effect of H_2O on liquidus phase relations in the haplogranite system at 2 and 5 kbar. Am Mineral 77: 1223–1241

Holtz F, Johannes W, Pichavant M (1992b) Peraluminous granites: the effect of alumina on melt composition and coexisting minerals. Trans R Soc Edinburgh Earth Sci 83: 409–416

Huppert HE, Sparks RSJ (1988) The generation of granitic magmas by intrusion of basalts into continental crust. J Petrol 29: 599–624

Johannes W (1978) Melting of plagioclase in the system Ab-An-H_2O and Qz-Ab-An-H_2O at PH_2O = 5 kbar: an equilibrium problem. Contrib Mineral Petrol 66: 295–303

Johannes W (1980) Metastable melting in the granite system Qz-Or-Ab-An-H_2O. Contrib Mineral Petrol 68: 221–330

Johannes W, Holtz F (1990) Formation and composition of H_2O-undersaturated granitic melts. In: Ashworth JR, Brown M (eds) High-temperature metamorphism and crustal anatexis. Mineral Soc Ser 2: pp 87–104

Joyce DB, Voigt DE (1994) A phase equilibrium study in the system $KAlSi_3O_8$-$NaAlSi_3O_8$-Al_2SiO_5-H_2O and petrogenetic implications. Am Mineral 79: 504–512

Laporte D (1994) Wetting behavior of partial melts during crustal anatexis: the distribution of hydrous silicic melts in polycrystalline aggregates of quartz. Contrib Mineral Petrol 116: 486–499

Laporte D, Orsini JB, Fernandez A (1991) Le complexe d'Ile Rousse, Balagne, Corse du Nord Ouest: pétrologie et cadre de mise en place des granites magnésio-potassiques. Geol Fr 4: 15–30

Le Breton N, Thompson AB (1988) Fluid-absent (dehydration) melting in metapelites in the early stage of crustal anatexis. Contrib Mineral Petrol 99: 226–237

Luth WC, Jahns RH, Tuttle OF (1964) The granite system at pressure of 4 to 10 kilobars. J Geophys Res 69: 759–773

Montel JM, Abdelghaffar A (1993) Les granites tardimigmatitiques du Velay (Massif Central français): principales caractéristiques pétrographiques et géochimiques. Géol Fr 1: 15–28

Montel JM, Marignac C, Barbey P, Pichavant M (1992) Thermobarometry and granite genesis: the Hercynian low-*P*, high-*T* Velay anatectic dome (French Massif Central). J Metamorphic Geol 10: 1–15

Nekvasil H (1988) Calculated effect of anorthite component on the crystallization paths of H_2O-undersaturated haplogranitic melts. Am Mineral 73: 966–981

Nekvasil H (1992) Ternary feldspar crystallization in high temperature felsic magmas. Am Mineral 77: 592–604

Nekvasil H, Burnham WC (1987) The calculated individual effects of pressure and water content on phase equilibria in the granite system. In: Mysen BO (ed) Magmatic processes: physicochemical principles. Geochem Soc Spec Publ 1, pp 433–445

Patiño-Douce AE, Johnston AD (1991) Phase equilibria and melt productivity in the pelitic system: implications for the origin of peraluminous granitoids and aluminous granulites. Contrib Mineral Petrol 107: 202–218

Patiño-Douce AE, Johnston AD, Rice JM (1993) Octahedral excess mixing properties in biotite: a working model with application to geobarometry and geothermometry. Am Mineral 78: 113–131

Peirera MD, Bea F (1994) Cordierite-producing reactions in the Pena Negra complex, Avila batholith, Central Spain: the key role of cordierite in low-pressure anatexis. Geochim Cosmochim Acta 32: 763–780

Provost A (1989) Block-wise global inversion. Terra Abstr 1: 328

Puziewicz J, Johannes W (1988) Phase equilibria and composition of Fe-Mg-Al minerals and melts in water-saturated peraluminous granitic systems. Contrib Mineral Petrol 100: 156–168

Puziewicz J, Johannes W (1990) Experimental study of a biotite-bearing granitic system under water-saturated and water-undersaturated conditions. Contrib Mineral Petrol 104: 397–406

Rapp RP, Watson EB, Miller CF (1991) Partial melting of amphibolite/eclogite and the origin of Archean trondhjemite and tonalite. Precambrian Res 51: 1–25

Robert JL (1976) Titanium solubility in synthetic phlogopite solid solutions. Chem Geol 17: 213–227

Rushmer T (1991) Partial melting of two amphibolites: contrasting experimental results under fluid absent conditions. Contrib Mineral Petrol 107: 41–59

Rutter MJ, Wyllie PJ (1988) Melting of vapour-absent tonalite at 10 kbar to simulate dehydration-melting in the deep crust. Nature 331, 6152: 159–160

Scaillet B, France-Lanord C, Le Fort P (1990) Badrinath-Gangotri plutons (Garwhal India): petrologogical and geochemical evidence for fractionation processes in a High Himalayan leucogranite. J Volcanol Geothermal Res 44: 163–188

Schreyer W, Maresch WV, Daniels P ,Wolfsdorff P (1990) Potassic cordierite: characteristic mineral for high-temperature, very low pressure environment. Contrib Mineral Petrol 105: 162–172

Seck HA (1971) Koexistierende Alkalifeldspäte und Plagioklase im System $NaAlSi_3O_8$-$KAlSi_3O_8$- $CaAl_2Si_2O_8$-H_2O bei temperaturen von 650 °C bis 900 °C. Neues Jahrb Mineral Abh 115: 315–345

Silver LT, Chappell BW (1988) The Peninsular Range Batholith: an insight into the evolution of the cordilleran batholiths of southwestern North America. Trans R Soc Edinburgh Earth Si 79: 105–121

Skjerlie KP, Johnston AD (1992) Vapor-absent melting at 10 kbar of biotite- and amphibole-bearing tonalic gneiss: implication for the generation of A-type granites. Geology 20: 263–266

Stern CR, Wyllie PJ (1981) Phase relationships of I-type granite with H_2O to 35 kbar. The Dinkey Lakes biotite granite from Sierra-Nevada batholith. J Geophys Res 86: 10412–10422

Thompson AB (1982) Dehydration-melting of pelitic rocks and the generation of H_2O-undersaturated granitic liquids. Am J Sci 282: 1567–1595

Tuttle OF, Bowen NL (1958) Origin of granite in the light of experimental studies in the system $NaAlSi_3O_8$-$KAlSi_3O_8$-SiO_2-H_2O. Geol Soc Am Mem 74

Vidal Ph, Cocherie A, Le Fort P (1982) Geochemical investigations of the origin of the Manaslu leucogranite (Hymalaya Nepal). Geochim Cosmochim Acta 46: 2279–2292

Vielzeuf D, Holloway JR (1988) Experimental determination of the fluid-absent melting relations in the pelitic system. Consequence for crustal differentiation. Contrib Mineral Petrol 98: 257–276

Vielzeuf D, Montel JM (1994a) Partial melting of metagreywackes. 1. Fluid-absent experiments and phase relationships. Contrib Mineral Petrol 117: 375–393

Vielzeuf D, Montel JM (1994b) Experimental constraints on partial melting in the crust. Mineral Mag 58A, 940–941

Vielzeuf D, Clemens JD, Pin C, Moinet E (1990) Granites, granulites, and crustal differentiation. In: Vielzeuf D, Vidal Ph (eds) Granulites and crustal evolution. NATO ASI Series, Kluwer Academic Publishers, pp 59–85

Vielzeuf D, Montel JM, Provost A, Kryza R (1991) The biotite-garnet-plagioclase-quartz assemblage as a potential geobarometer (abstract). EOS Trans AM Geophyc Union 72, 44: 559

White AJR, Chappell BW (1988) Some supracrustal (S-type) granites of the Lachlan Fold Belt. Trans R Soc Edinburgh Earth Sci 79: 169–181

Winkler HGF (1957) Experimentelle Geisteinsmetamorphose.-I. Hydrothermale Metamorphose karbonatfreier Tone. Geochim Cosmochim Acta 13: 42–69

Wyart J, Sabatier G (1959) Transformation des sédiments pélitiques à 800 °C sous une pression d'eau de 1800 bars et granitisation. Bull Soc Fr Minéral Cristallogr 82: 201–210